Utrecht University

Department of Physics

Bachelor Thesis

Ima Meijer

Porosity optimization of nanoscale membranes

Supervisors:

Prof. dr. R. van Roij
Institute for Theoretical Physics

MSc. W. Boon
Institute for Theoretical Physics

12 June 2019

Abstract

In this thesis fluid fluxes and electric charge fluxes as a result of a pressure gradient, electric field or salt concentration gradient, through a nanopore with a charged surface, are considered. It is found that the fluxes react linearly to the considered driving forces. Every driving force induces not only its conjugate flux but also all other Fluxes. By solving the Poisson-Nernst-Planck-Stokes equations numerically, fluxes as a result of salt concentration gradient driven flow through a chain of nanopores, a membrane, can be simulated. From these simulations an optimal geometry is found to maximixe the generated power per unit volume membrane.

Contents

1 Introduction

Energy can be harvested from adding salt water to fresh water. This way of generating electricity is called blue energy. When adding salt water to fresh water, the salt water will diffuse throughout the fresh water. This diffusive effect makes for a salt flux going from high salt concentrations to low salt concentrations. This flux of ions, which is nothing more than an electric current, can be used to generate electricity. But plainly adding salt water to fresh water does not generate any electricity that can be harvested. Swimming from a river into the sea, will not let anyone swim faster because of any released energy. A way to actually harvest this energy, is to separate the salt and fresh water by a membrane. Due to the presence of an electrical double layer (EDL) in the pore of the membrane, a net charge flux, an electric current, is then developed through the pore of the membrane. The EDL is a layer that is present on a length scale, depending on the bulk ion concentration, is in the order of nanometers, therefore the pores in the membranes used, are also in the order of nano- to micrometers to maximize efficiency [1]. When incorporating the membrane into a closed electrical circuit. The chemical energy from the difference in salt concentration can be converted into electrical energy. This process is called reversed electrodialysis (RED) [2]. Unfortunately the efficiency of current harvesting techniques is currently too low to compete with wind- and solar energy [3]. Blue energy has the potential to be a significant contributor to the current energy problem. All around the world, where rivers are entering the sea, potential energy is lost. Estimates suggest that more than 1TW of energy can be harvested worldwide, which is the equivalent of around 1000 nuclear reactors [4]. To make the process of RED as efficient as possible, it is required to know how the induced fluid flow and the induced ion flow through a nanopore exactly work. How do these fluxes react to changes in salt concentration? How do these fluxes react to different kinds of porosity (measure of the distribution of holes in a membrane) of the membrane? It is the goal of this thesis to gain insight on the processes playing a role in RED, with which in the end recommendations can be done for an optimal membrane. These investigations are purely geometrical and do not touch on any chemical properties of the material of the membrane such as [3] or [5]. Moreover the shape of the pore considered is straight and not conical, bullet shaped or trumpet-shaped as in [6]. The distance between and the length of the pores will be the main variable considered. In the theory section of this thesis, the electric double layer (EDL) is discussed. Furthermore a salt concentration gradient in interaction with this EDL as a driving force behind fluid fluxes and electrical currents (net charge flux from ion flow) is discussed, but also a pressure gradient and an electric field as a driving force is considered. It turns out that there is a linear relation between these driving forces and the resulting fluxes. Finally a numerical model is used to find an ideal porosity to maximize induced fluxes as a result of a salt concentration gradient.

2 Theoretical background

In this section the theoretical background to understand flow through a channel such as a nanopore, is given. Three driving forces are considered, namely: a pressure gradient, an electric field and a salt concentration gradient. The fluid volume flux and the net charge

flux, or electric current, are the fluxes generated by these driving forces and are derived in this section. A single driving force, always induces a fluid volume flux as well as an electric current, but also other fluxes that are beyond the scope of this thesis such as, e.g. a salt flux or a heat flux.

2.1 Navier-Stokes equation

Before discussing fluid flow through a channel, resembling the fluid flow through a nanopore, it is important to be able to describe fluid flow in general. The Navier-Stokes equation is, together with the mass continuity equation, the governing equation for incommpressible laminar fluid flow. In this section the Navier-Stokes equation for incompressible fluids is derived from the integral momentum balance. This equation is then solved for cases, versions of which are encountered later again in this thesis. This section mostly follows the discussion of van Heijst [10].

Before the integral momentum balance is considered to derive the Navier-Stokes equation, first consider the relation

$$\frac{\partial}{\partial t}\iiint_V \rho dV = -\iint_S (\rho\vec{u})\cdot\hat{n}dS \tag{2.1}$$

which describes conservation of mass, where ρ is the mass density of the fluid, $\vec{u}$ the velocity of the fluid element dV and $\hat{n}$ the normal to the surface element dS. This relation states that the change of mass within the volume V is given by the surface integral of the flux of mass going in- or out of the surface of the volume. So any change of mass within a volume is due to an in- or outgoing mass flux to or from that volume. For an incompressible fluid, ρ is constant and thus $\partial\rho/\partial t = 0$. Combined with the divergence theorem this gives

$$\nabla\cdot\vec{u} = 0, \tag{2.2}$$

which is the continuity equation for incompressible fluid flow [13].
Now consider a volume element dV, the momentum of its mass is $\rho\vec{u}dV$ with ρ the mass density of the fluid and $\vec{u}$ the velocity of the fluid element. The increase of the total momentum of the mass in the volume V per unit time is

$$\frac{\partial}{\partial t}\iiint_V \rho\vec{u}dV, \tag{2.3}$$

this increase can either be a consequence of flux of mass through the surface S (boundary of V) or of forces doing work on the fluid element. The total rate of incoming momentum flux through the surface S with normal $\hat{n}$ of surface element dS can be written as

$$-\iint_S \rho\vec{u}(\vec{u}\cdot\vec{n})dS. \tag{2.4}$$

These equations can be combined into the momentum balance

$$\frac{\partial}{\partial t}\iiint_V \rho\vec{u}dV + \iint_S \rho\vec{u}(\vec{u}\cdot\vec{n})dS = \sum F. \tag{2.5}$$

This can be seen as a version of Newton's second law. The net momentum increase per unit time of the mass inside V, together with the net outward flux of the momentum through the surface S, are equal to the sum of all forces $\sum$F acting on the mass inside V. The sum of all forces consists of body forces acting on every element dV inside V and of surface forces acting on the surface elements dS. The surface forces can be divided into tension normal to the surface (such as pressure) and shear stress tension parallel to the surface. The total sum of surface forces acting on a surface element dS will be denoted by $\vec{t}dS$, which can de written as $\vec{t} = \hat{n} \cdot \boldsymbol{\sigma}$, for surfaces with outward normal $\hat{n}$. Here $\boldsymbol{\sigma}$ represents the stress tensor, which completely defines the state of stress inside the fluid volume V (note that the bold notation is used to denote second-rank tensors). Every fluid element feels these normal and shear stresses from neighbouring fluid elements but exerts these same forces on its own neighbouring fluid parcels, such that these tensions are present everywhere in the volume V. The sum of forces can be written as:

$$\sum F = \iiint_V \rho \vec{g} dV + \iint_S \boldsymbol{\sigma} \cdot \hat{n} dS, \tag{2.6}$$

with $\vec{g}$ being the acceleratoin due to a body force acting on the fluid element dV. The expressions for $\sum F$ from (2.5) and (2.6) can be combined, to yield:

$$\frac{\partial}{\partial t} \iiint_V \rho \vec{u} dV + \iint_S \rho \vec{u} (\vec{u} \cdot \vec{n}) dS = \iiint_V \rho \vec{g} dV + \iint_S \boldsymbol{\sigma} \cdot \hat{n} dS. \tag{2.7}$$

Making use of the divergence theorem and taking the derivative with respect to time of the first term now yields:

$$\iiint_V \left[\rho \frac{\partial \vec{u}}{\partial t} + \vec{u} \frac{\partial \rho}{\partial t} + \vec{u} \nabla \cdot (\rho \vec{u}) + \rho (\vec{u} \cdot \nabla) \vec{u} \right] dV = \iiint_V \left[\rho \vec{g} + \nabla \cdot \boldsymbol{\sigma} \right] dV. \tag{2.8}$$

The second and third term of the left-hand side of equation (2.8) vanish for incompressible media following from the mass continuity equation that states that the rate of mass entering a system is equal to the rate of mass leaving the system plus any accumulation of mass within the system, see equation (2.2). Since an arbitrary volume V is considered, the integrand from both sides of the above equation must be zero yielding:

$$\frac{\partial \vec{u}}{\partial t} + (\vec{u} \cdot \nabla) \vec{u} = \vec{g} + \frac{1}{\rho} \nabla \cdot \boldsymbol{\sigma}. \tag{2.9}$$

As discussed previously, the stress tensor consists of all the stress components working on the fluid, consisting of viscous (parallel to the surface) and non-viscous (normal to the surface) components. Thus the stress tensor can be decomposed as:

$$\boldsymbol{\sigma} = -p\mathbf{1} + \boldsymbol{\tau}, \tag{2.10}$$

with $\mathbf{1}$ being the unity matrix, $\boldsymbol{\tau}$ representing the viscous shear stress and p the pressure. From experimental observation it is known that dense liquids such as water can be treated as a Newtonian fluid. For a Newtonian fluid the viscous stress at every point is linearly

proportional to the rate of change of its velocity vector going from that point outward in all directions[1]. A relation for the viscous stress tensor is now obtained as:

$$\frac{1}{\rho}\nabla\tau = \frac{\eta}{\rho}\nabla^2\vec{u} \equiv \nu\nabla^2\vec{u}, \tag{2.11}$$

with η being the dynamic viscosity, which is a measure of the resistance of the fluid to deformation caused by shear stress and $\nu \equiv \eta/\rho$ the kinematic viscosity. Combining equation (2.9),(2.10) and (2.11) yields the Navier-Stokes equation for incompressible media:

$$\frac{\partial\vec{u}}{\partial t} + (\vec{u}\cdot\nabla)\vec{u} = -\frac{1}{\rho}\nabla p + \nu\nabla^2\vec{u} + \vec{g}. \tag{2.12}$$

Note this equation balances forces per unit mass density, to get real forces one most multiply the above equation by ρ. Together with the continuity equation $\nabla\vec{u} = 0$ these are four equations with four unknowns. So with the appropriate boundary conditions this is a closed set of equations. The length scales considered in this thesis are such that the Reynolds number is much smaller than one [16]. This reduces the Navier-Stokes equation (2.12) to:

$$\rho\frac{\partial\vec{u}}{\partial t} = -\nabla p + \eta\nabla^2\vec{u} + \vec{f} \tag{2.13}$$

and is called the Stokes equation. Here $\vec{f}$ is now the body force per unit volume.

2.2 Plane Poiseuille flow

The Navier-Stokes equation (2.12) can now be used to describe fluid flow between two plates called plane Poiseuille flow. Consider two parallel plates stretched out in the x-direction with length L at $z = 0$ and $z = H$, with $L \gg H$, translational invariant in the y-direction under influence of an applied pressure gradient in the x-direction $((dp/dx), 0, 0)$. It is assumed the flow is fully developed and stationary, meaning the velocity is only dependent on the vertical coordinate and all time derivatives vanish. From the continuity equation immediately follows:

$$\frac{\partial u_x}{\partial x} + \frac{\partial u_z}{\partial z} = 0 \Rightarrow \frac{\partial u_z}{\partial z} = 0. \tag{2.14}$$

Together with the boundary condition $u_z(z = 0) = 0$ it follows that $u_z = 0$ for the whole considered region. The fluid must have one velocity component, namely its component in the x-direction which is only dependent on the z-coordinate. The x and z component of the Navier-Stokes equations now reduce to:

$$\frac{1}{\rho}\frac{\partial p}{\partial x} = \nu\frac{\partial^2 u_x}{\partial z^2}; \tag{2.15}$$

$$\frac{1}{\rho}\frac{\partial p}{\partial z} = 0. \tag{2.16}$$

[1]For a detailed derivation see section 2.4 of van Heijst [10]

Here it is assumed that there are no other external body forces, i.e. it is assumed the gravitational force is negligible, such that $\frac{\partial p}{\partial z} = 0$. This means the pressure is not z-dependent but only depends on the x-coordinate: $p(x)$.
The velocity profile can be evaluated by integrating equation (2.15) twice (notice the ν absorbing the ρ to become η):

$$u_x(z) = \frac{z^2}{\eta}\frac{dp}{dx} + C_1 z + C_2, \tag{2.17}$$

where the x subscript denotes the velocity direction. Applying no slip boundary conditions, $u(0) = u(H) = 0$ yields

$$u_x(z) = -\frac{1}{2\eta}\frac{dp}{dx} z(H - z), \tag{2.18}$$

which is a parabolic velocity profile. The fluid particles only move parallel to each other in layers. This is called laminar flow or plane Poiseuille flow. Laminar flow through a cylindrical pipe is called Poiseuille flow and is discussed in the appendix. The fluid volume flux in the x-direction, per unit length in the y-direction, is given by:

$$Q_u = \int_0^H u(z)dz = -\frac{1}{12}\frac{1}{\eta}\frac{dp}{dx}H^3. \tag{2.19}$$

It will be very instructive to compare the volume fluxes of the different set ups we will be looking at later in this thesis to the hydraulic volume flux, i.e. the volume flux of the Poiseuille flow obtained here, because it can be a measure of the efficiency of the fluid transport of the configuration considered. From the volume flux the average velocity in the channel follows

$$\overline{u}_x = \frac{Q_u}{H} = -\frac{1}{12}\frac{1}{\eta}\frac{dp}{dx}H^2. \tag{2.20}$$

With this result we are now able to write the velocity distribution in terms of the average velocity

$$u_x(z) = 6\overline{u}_x \frac{z}{H}(1 - \frac{z}{H}), \tag{2.21}$$

from which follows that the maximum velocity in the channel is right in the middle at $z = H/2$ and equals $(3/2)\overline{u}_x$.

2.3 Boundary layer in a solvent (Electric double layer)

In this section the behaviour of an external object immersed in water is studied, mainly following the discussion by van Roij [12]. This object could be a macroscopic glass surface, a colloidal particle or a microscopic nanopore. The relatively large dielectric constant of water ($\epsilon_{water}/\epsilon_{air} \simeq 80$), means that the chemical groups on the surface of the considered object have the tendency to dissociate. Free ions will leave the surface. This presence of free ions in the water can be explained by the competition between ionic entropy and electrostatic energy. The ions in the solvent have the natural tendency to be homogeneously distributed in space while ions of opposite charge are attracted to each other. Now because these free ions have left the surface, a net charge on the surface is established. This net charge is then

screened by counter-ions (ions of opposite charge to the surface charge) that are attracted to the surface. Thus in the region close to the surface there is a charge imbalance. This region is called the Debye layer. The closer to the surface the more counter-ions that are attracted to the surface and the larger the electric potential resulting from this charge imbalance. Eventually an equilibrium is created called the electric double layer (EDL).

Now consider a homogeneous surface of macroscopic area A in the plane $z = 0$. The surface is in contact with a solvent of dielectric constant ϵ and temperature T in the volume $z > 0$ in which monovalent cations and anions of charge $\pm e$, with e the elementary charge, are dissolved. The concentration far from the surface (bulk concentration) is $2\rho_b$. The volume $z < 0$ is a conducting solid medium at a constant electric potential. It is known that the chemical groups on the surface of the object will release free ions leading to a net surface charge of $e\rho_s$ homogeneously distributed over the surface. The characteristics of the established electric double layer can be found using the Poisson equation, which describes the spatially changing electrical potential in the solvent due to excess charge. For $z > 0$ this becomes

$$\frac{d^2\psi(z)}{dz^2} = -\frac{e}{\epsilon_0\epsilon}\left(\rho_+(z) - \rho_-(z)\right), \tag{2.22}$$

where $\psi(z)$ is the electrostatic potential and $e\left(\rho_+(z) - \rho_-(z)\right)$ can be recognized as the ionic charge density $e\rho_e(z)$. The energy of an ion with charge $\pm e$ at position z is given by its electrostatic energy $\pm e\psi(z)$, which plugged in to the Boltzmann equation gives

$$\rho_\pm = \rho_b \exp[\mp\beta e\psi(z)], \tag{2.23}$$

where $\beta^{-1} = k_\mathrm{B}T$, with k_B the Boltzmann constant. Together equation (2.22) and (2.23) now yield the Poisson-Boltzmann equation

$$\frac{d^2\psi(z)}{dz^2} = \frac{e}{\epsilon_0\epsilon}\rho_b\left(e^{\beta e\psi(z)} - e^{-\beta e\psi(z)}\right) = \frac{2e}{\epsilon_0\epsilon}\rho_b \sinh(\beta e\psi(z)). \tag{2.24}$$

Now introducing the dimensionless electric potential $\phi(z) = \frac{e\psi(z)}{k_\mathrm{B}T}$ to find the expression

$$\frac{d^2\phi(z)}{dz^2} = \kappa^2 \sinh(\phi(z)), \tag{2.25}$$

with $\kappa^2 = \frac{2e^2}{\epsilon_0\epsilon k_\mathrm{B}T}\rho_b$. The relation $\rho_\pm(z \to \infty) = \rho_b$ must always hold, which results in the first boundary condition to this second-order differential equation

$$\lim_{z\to\infty} \phi(z) = 0. \tag{2.26}$$

The second boundary condition comes from the fact that the total ionic charge in the solvent must be exact the opposite of the total charge on the surface. Because the surface charge is homogeneously distributed, $e\rho_s$ must be equal and opposite to the ionic charge density times e integrated over z from anywhere along the surface:

$$e\rho_s = -e\int_0^\infty dz\rho_e(z) = \epsilon_0\epsilon\int_0^\infty dz\frac{d^2\psi(z)}{dz^2} = -\epsilon_0\epsilon\frac{d\psi(0^+)}{dz} \tag{2.27}$$

$$\Rightarrow \rho_s = -\left(\frac{\epsilon_0 \epsilon k_\mathrm{B} T}{e^2}\right) \frac{d\phi(0^+)}{dz}, \tag{2.28}$$

it can now be deduced that

$$\frac{d\phi(0^+)}{dz} = -\left(\frac{e^2}{\epsilon_0 \epsilon k_\mathrm{B} T}\right) \rho_s \equiv -4\pi \lambda_\mathrm{B} \rho_s, \tag{2.29}$$

where λ_B is defined as the Bjerrum length which together with the Debye length κ^{-1} are two important length scales regarding the electrical double layer:

$$\lambda_\mathrm{B} = \frac{e^2}{4\pi \epsilon_0 \epsilon k_\mathrm{B} T}, \tag{2.30}$$

$$\kappa^{-1} = \left(\frac{2e^2 \rho_b}{\epsilon_0 \epsilon k_\mathrm{B} T}\right)^{-1/2} = \frac{1}{\sqrt{8\pi \lambda_\mathrm{B} \rho_b}}. \tag{2.31}$$

The Bjerrum length λ_B can be seen as the length along which the Coulomb interaction potential equals $k_\mathrm{B}T$ (for interactions between two dissolved unit charges e) which can be seen when we write it in the following way

$$\frac{e^2}{4\pi \epsilon_0 \epsilon r} = \frac{\lambda_\mathrm{B} k_\mathrm{B} T}{r} \tag{2.32}$$

The Debye length κ^{-1} can be seen as the length scale over which charge imbalance can persist. Keep in mind that these length scales are derived for monovalent ions only and will not be the same for all higher valent ions.
The established second-order differential equation together with the two boundary conditions can in principle now be solved. The full equation with its boundary conditions is:

$$\frac{d^2\phi(z)}{dz^2} = \kappa^2 \sinh(\phi(z)), \tag{2.33}$$

$$\lim_{z\to\infty} \phi(z) = 0, \tag{2.34}$$

$$\frac{d\phi(0^+)}{dz} = -4\pi z_s \lambda_\mathrm{B} \rho_s, \tag{2.35}$$

which can be solved and has solution (ref?):

$$\phi(z) = 2 \ln \frac{1 + \gamma \exp[-\kappa z]}{1 - \gamma \exp[-\kappa z]}, \tag{2.36}$$

with γ an integration constant fixed by:

$$\frac{4\gamma}{1-\gamma^2} = \frac{4\pi z_s \lambda_\mathrm{B} \rho_s}{\kappa} \equiv y, \tag{2.37}$$

when y is defined as above γ becomes

$$\gamma = \frac{\sqrt{1 + (y/2)^2} - 1}{y/2} = \begin{cases} y/4 & \text{if } |y| \ll 1 \\ 1 & \text{if } |y| \gg 1. \end{cases} \tag{2.38}$$

Equation 2.36 can be Taylor-expanded for large z to give:

$$\phi(z) \simeq 4\gamma \exp[-\kappa z] \tag{2.39}$$

such that the electrostatic potential in its far-field asymptotic form looks like:

$$\phi(z) = \begin{cases} y\exp[-\kappa z] & \text{if } |y| \ll 1 \\ 4\exp[-\kappa z] & \text{if } |y| \gg 1. \end{cases} \tag{2.40}$$

2.4 Nernst-Planck equation

Before interaction of the electric double layer with fluid flow due to external driving forces is considered, first expressions for the different particle fluxes (or currents) that can arise are derived. The particle flux density of species i, $\vec{J}_i(\vec{r})$, can be decomposed into an advective component and a component that can be directly derived from Fick's law, that gives both the diffusive and conductive components

$$\vec{J}_i = \vec{J}_i^{\text{Fick}} + \vec{J}_i^{\text{adv}}. \tag{2.41}$$

Relations for the non-advective flux densities can be found from Fick's law. Fick's law is an empirical law found by Fick [15], which states that a particle flux goes from regions of high concentration to regions of low concentration and is based on the conservation of species

$$\vec{J}_i^{\text{Fick}} = -D_i \frac{\rho_i}{k_\text{B}T} \nabla \mu. \tag{2.42}$$

Here D_i is the diffusion constant of species i, $\rho_i(\vec{r})$ the particle density of species i and μ is the chemical potential of the species. The $k_\text{B}T$ term comes from the Nernst-Einstein relation[2]. Combining this with the definition of the chemical potential from the Gibbs free energy[3]

$$\mu = \left(\frac{dG}{dN}\right)_{P,T} = k_\text{B}T \ln \rho_i - z_i e \psi, \tag{2.43}$$

where the Gibbs free energy is that of an ideal gas with an external field with potential $\psi(\vec{r})$, now gives

$$\vec{J}_i^{\text{Fick}} = -D_i \rho_i \nabla \ln \rho_i + D_i \frac{\rho_i}{k_\text{B}T} z_i e \nabla \psi = -D_i \nabla \rho_i + D_i \frac{\rho_i}{k_\text{B}T} z_i e \nabla \psi \tag{2.44}$$

The first term now describes the diffusion of the particle concentration, the fluid always strives to maximize its entropy by initiating a particle flux from high to low concentration. The second term describes conduction of the particles, that the diffusing particles are moved with respect to the fluid by the external electrostatic field [13].
The advective flux density comes from the particle flux due to the fluid flow and therefore is given by the fluid flow velocity field times the particle concentration of the species

$$\vec{J}_i^{\text{adv}} = \rho_i \vec{u}(\vec{r}). \tag{2.45}$$

[2] See chapter 11 from Kirby [13] for a detailed discussion.
[3] See chapter 10 from Kirby [13] for a detailed discussion.

The diffusive, conductive and advective flux densities can now be combined to give the total particle flux density

$$\vec{J}_i = -D_i\left(\nabla\rho_i - \frac{\rho_i}{k_\mathrm{B}T}z_i e\nabla\psi\right) + \rho_i\vec{u} \tag{2.46}$$

and together with the relation between the particle flux density and the particle density that can be found from the continuity of particle number equation, that is found in the same way as (2.2)

$$\nabla\cdot\vec{J}_i = -\frac{\partial\rho_i}{\partial t}, \tag{2.47}$$

the particle flux density can be described. Equation (2.46) is called the Nernst-Planck equation and describes the motion of a charged species in a fluid. The Nernst-Planck equation together with the continuity equation (2.47), Poisson equation (2.22) and the Stokes equation (2.13) are called the Poisson-Nernst-Planck-Stokes (PNPS) equations. The PNPS equations can be used to describe the fluid and (charged) particle flow through a nanopore. In the following sections they will be used to consider different kind of flows, i.e. flows induced by different driving forces.

2.5 Streaming current

The physics of the electric double layer, the hydraulically driven flow through a bounded region and the different currents that can arise have now been considered. These can be combined to see what happens if a pressure driven flow flows through a region with a net charge. Consider again our setup of two parallel plates stretched out in the x direction with length L at $z = 0$ and $z = H$, with translational invariance in the y-direction under influence of an artificial pressure gradient in the x-direction. With fully developed and stationary flow. In section 2.3 it has been explained that there must be a net charge in the region $0 < z < \kappa^{-1}$. The induced flow drives a net advective charge flux I_adv which is nothing else than net electric current, also called the streaming current. The streaming current in the x-direction per unit length in the y-direction for the outlined configuration is

$$I_\mathrm{adv} = 2e\int_0^{H/2} dz\left(\vec{J}_+^{\mathrm{adv}} - \vec{J}_-^{\mathrm{adv}}\right) = 2e\int_0^{H/2} dz\rho_e(z)u_x(z), \tag{2.48}$$

it can now be noted that only the advective term from the Nernst-Planck equation contributes to the current, all other terms vanish since there is no electric field or salt concentration gradient. The ionic charge density $e\rho_e(z)$ can now be rewritten using the Poisson-Boltzmann equation (2.22) and the velocity profile is given by the linear term from (2.18) since there is only a net charge in the EDL, there is only a streaming current for $z < \kappa^{-1} \ll H$, the streaming current in the x-direction per unit length in the y-direction now becomes

$$I_\mathrm{adv} = \frac{\epsilon_0\epsilon}{\eta}\frac{dp}{dx}H\int_0^{H/2} dzz\frac{d^2\psi(z)}{dz^2} = -\frac{\epsilon_0\epsilon}{\eta}\frac{dp}{dx}H\int_0^{H/2} dz\frac{d\psi(z)}{dz} = \frac{\epsilon_0\epsilon}{\eta}\frac{dp}{dx}H\psi(0), \tag{2.49}$$

where the potential vanishes at $z = H/2$ (outside the EDL) and integration by parts is used to evaluate the integral. If an overlapping EDL is considered the potential does not vanish at $z = H/2$ and an extra term is to be added in the expression for the streaming current.

2.6 External electric field

The effect of an external electric field on an electrolyte between two homogeneously charged surfaces at $z = 0$ and $z = H$ can also be studied. Consider again the setup from section 2.3, the so called electrical double layer. The fluid flow is now governed by the Stokes equation (2.13). To know what happens if a constant electric field in the x-direction is switched on, known as electro osmosis (EO). The electric field works as a body force on the charged particles in the solute. Therefore the body force is a product of the local charge and local electric field such that $\vec{f} = -e\sum_i z_i\rho_i(\vec{r},t)\nabla\psi(\vec{r},t)$, with ρ_i the local electric charge density, z_i the charge valency of the considered particle and all other parameters as defined earlier. The initial state of the fluid is stationary, if an electric field is switched on, qualitatively, the fluid begins to move and $\partial\vec{u}/\partial t$ is not zero anymore, just as ∇p does not necessarily have to be zero. But eventually the equilibrium state is reached and the system is stationary again, making the time derivatives vanish as well as the pressure gradient. From now on, only this stationary equilibrium state will be considered. For a large reservoir with constant pressure, the pressure term vanishes as well, which simplifies the equation of motion to

$$0 = \eta\nabla^2\vec{u} - \epsilon_0\epsilon(\nabla^2\psi(z))\vec{E}, \tag{2.50}$$

where the Poisson-Boltzmann equation is used (2.22) to simplify $\vec{f}$. If the electric field and thus the velocity is just in the x-direction: $\vec{E} = (E_x, 0, 0)$ and $\vec{u} = (u_x(z), 0, 0)$. The direction has not been specified yet, the velocity and the electric field can still be in either the positive or negative direction. The Stokes equation is reduced to just the x-component of equation (2.50)

$$\eta\frac{d^2u_x(z)}{dz^2} = \epsilon_0\epsilon E_x\frac{d^2\psi(z)}{dz^2}. \tag{2.51}$$

Integrating twice gives as a general solution

$$\eta u_x(z) = \epsilon_0\epsilon E_x\psi(z) + C_1 z + C_2, \tag{2.52}$$

with integration constants C_1 and C_2. Using the no-slip boundary conditions $u_x(0) = u_x(H) = 0$ and realizing $\psi(H) = \psi(0)$ by virtue of symmetry, the velocity field becomes

$$u_x(z) = \frac{\epsilon_0\epsilon E_x}{\eta}\Big(\psi(z) - \psi(0)\Big). \tag{2.53}$$

Here it can be seen that the vertical length the velocity needs, to reach its maximum velocity, is given by the Debye length κ^{-1}, since the potential vanishes outside the Debye layer. For the remainder of the channel the velocity is constant and maximum, i.e. $u_x(z)$ is maximum for $\kappa^{-1} < z < H - \kappa^{-1}$ and since $H \gg \kappa^{-1}$ it follows $u_{xmax}(z) \approx \overline{u}_x$. For $z \gg \kappa^{-1}$ the velocity profile is given by

$$u_x(z) = -\frac{\epsilon_0\epsilon E_x}{\eta}\psi(0) = u_{xmax}(z) \approx \overline{u}_x. \tag{2.54}$$

It can be seen that the maximum velocity is reached in almost the entire channel, only in the regions in the order of a Debye length close to the surface the fluid is slowed down due to the presence of the surface. In contrast to the parabolic velocity profile of the hydraulically

driven Poiseuille flow, where the fluid is slowed down by the surface across the entire channel. The fluid volume flux in the x-direction, per unit length in the y-direction is given by

$$Q_u = \overline{u}_x H = -\frac{\epsilon_0 \epsilon E_x H}{\eta}\psi(0). \tag{2.55}$$

The current, due to velocity field (advective charge flux), in the x-direction per unit length in the y-direction due to an external electric field therefore is again given by equation (2.48) and becomes using equation (2.53)

$$\begin{aligned} I_{\text{adv}} &= -\frac{2E_x\epsilon_0^2\epsilon^2}{\eta}\left[\psi(0)\frac{d\psi(0)}{dz} + \int_0^{H/2}\frac{d^2\psi(z)}{dz^2}\psi(z)dz\right] \\ &= -\frac{2E_x\epsilon_0^2\epsilon^2}{\eta}\left[\psi(0)\frac{d\psi(0)}{dz} + \int_0^{H/2} dz\left(\frac{d}{dz}\left(\frac{d\psi(z)}{dz}\psi(z)\right) - \left(\frac{d\psi(z)}{dz}\right)^2\right)\right] \\ = -\frac{2E_x\epsilon_0^2\epsilon^2}{\eta}&\left[\psi(0)\frac{d\psi(0)}{dz} - \frac{d\psi(0)}{dz}\psi(0) - \int_0^{H/2} dz\left(\frac{d\psi(z)}{dz}\right)^2\right)\Bigg] = \frac{2E_x\epsilon_0^2\epsilon^2}{\eta}\int_0^{H/2} dz\left(\frac{d\psi(z)}{dz}\right)^2. \end{aligned} \tag{2.56}$$

Here $\frac{d\psi(H/2)}{dz} = 0$ is used. The Poisson-Boltzmann equation (2.25) can now be used to find an integral that can be evaluated

$$\begin{aligned} \frac{d^2\phi(z)}{dz^2} &= \kappa^2\sinh(\phi(z)) \\ \frac{d\phi(z)}{dz}\frac{d^2\phi(z)}{dz^2} &= \kappa^2\frac{d\phi(z)}{dz}\sinh(\phi(z)) \\ \frac{1}{2}\frac{d}{dz}\frac{d^2\phi(z)}{dz^2} &= \kappa^2\frac{d}{dz}\cosh(\phi(z)) \\ \frac{1}{2}\left(\frac{d\phi(z)}{dz}\right)^2 &= \kappa^2\Big(\cosh(\phi(z)) + C\Big). \end{aligned} \tag{2.57}$$

Now since $\frac{d\psi(H/2)}{dz} = 0$ and $\phi(H/2)$ can always be shifted such that it vanishes, the integration constant is found as $C = -1$. The expression can now be plugged into equation (2.56) to yield

$$\frac{4\beta^2 e^2 E_x\epsilon_0^2\epsilon^2}{\eta}\int_0^{H/2} dz\kappa^2(\cosh(\phi(z)) - 1) = \frac{8\beta^2 e^2 E_x\epsilon_0^2\epsilon^2\kappa}{\eta}(\cosh(\phi(0)/2) - 1) \tag{2.58}$$

This time though, the electric field contributes to the charged particle flux as well. This contribution to the current in the x-direction per unit length in the y-direction can be found by integrating the conductive particle flux density over the channel height.

$$I_{\text{cond}} = 2E_x e^2\beta\int_0^{H/2} dz(D_+\rho_+ - D_-\rho_-), \tag{2.59}$$

where it is assumed there is no density gradient of the diluted ions and that the electric field only has a component in the x-direction. Since $D_+ = D_- = D$ and since the surface charge must be entirely screened by oppositely charged ions the integral reduces to

$$I_{\text{cond}} = 2E_x e^2\beta D\int_0^{H/2} dz(\rho_+ - \rho_-) = -2E_x e^2\beta D z_s\rho_s, \tag{2.60}$$

where z_s is the sign of the surface charge ρ_s. Now combining (2.58) and (2.60), the expression for the total charge flux now becomes

$$I = I_{\text{adv}} + I_{\text{cond}} = \frac{8\beta^2 e^2 E_x \epsilon_0^2 \epsilon^2 \kappa}{\eta}(\cosh(\phi(0)/2) - 1) - 2E_x e^2 \beta D z_s \rho_s. \tag{2.61}$$

2.7 External salt concentration gradient

Now consider again the same set up of the electrolyte between two homogeneously charged surfaces, but now with a difference in salt concentration between the two reservoirs, or diffusio-osmosis (DO). The chemical potential gradient $\nabla\mu$ resulting from the difference in salt concentration is now the driving force. Again it is to be expected that not only a salt flux is the result of this driving force but also a fluid volume flux as well as an electric current. The Navier-Stokes equation (2.12) in this case reduces to

$$\eta\nabla^2\vec{u} = \nabla p + \vec{f}. \tag{2.62}$$

With as body force now $\vec{f} = e\sum_i z_i\rho_i(\vec{r},t)\nabla\psi(\vec{r},t)$. This is the interaction between the salt ions and the surface charge. Note that this force is purely directed in the z-direction, $\psi(z)$ is the potential from the EDL. Together with the Boltzmann equation for a 1:1 electrolyte (2.23), (2.62) becomes

$$\eta\nabla^2\vec{u} = \nabla p - 2k_{\text{B}}T\rho_b(x)\sinh(\phi(z))\frac{d\phi(z)}{dz}\hat{k}. \tag{2.63}$$

Where $\hat{k}$ is the unit vector in the z-direction. Note that the body force resulting from the EDL potential is in the z-direction only. The bulk density is now dependent on the x-coordinate since there is no constant salt concentration along the channel length anymore. The fluid velocity also only has a component in the x-direction for an infinitely long channel with charged surfaces. Realizing this, the differential equation that is left for the pressure can now be solved

$$\frac{dp}{dz} = 2k_{\text{B}}T\rho_b(x)\frac{d}{dz}\Big(\cosh(\phi(z))\Big), \tag{2.64}$$

using the boundary condition that at $\phi(H/2)$, so outside the EDL, the potential drops to zero and that the pressure must be constant, $p = p_0$, the following expression for $p(x,z)$ can be found

$$p(x,z) = p_0 - 2\rho_b(x)k_{\text{B}}T(\cosh(\phi(z)) - 1). \tag{2.65}$$

Plugging this result back into (2.63) gives a differential equation for $\vec{u}$

$$\eta\frac{d^2u_x(z)}{dz^2} = 2k_{\text{B}}T(\cosh(\phi(z)) - 1)\frac{d\rho_b(x)}{dx}. \tag{2.66}$$

Note that the z-components all cancel, leaving only the x-component of the equation. This means that a concentration gradient along a charged surface induces a pressure gradient that cancels the body force due to the potential from the EDL, but since there is a concentration gradient and thus the bulk concentration is dependent on the x-coordinate, a pressure gradient in the x-direction is induced, resulting in fluid flow! An external salt concentration

gradient, thus, does not directly induce a fluid flow, there is no body force directly proportional to the fluid flow, but it does indirectly induce another driving force, namely a pressure gradient along the channel, that does directly induce a fluid flow. The differential equation for $\vec{u}$ can be integrated twice to give the velocity profile. To perform the first integral it is now convenient to rewrite the differential equation using the solution of the EDL potential (2.36)

$$\left.\begin{aligned} 2(\cosh(\phi(z))-1) \\ \phi(z) = 2\ln\frac{1+\gamma\exp[-\kappa z]}{1-\gamma\exp[-\kappa z]} \end{aligned}\right\} \Rightarrow 2(\cosh(\phi(z))-1) = 4\gamma e^{-\kappa z}\left(\frac{1}{(1-\gamma e^{-\kappa z})^2}-\frac{1}{(1+\gamma e^{-\kappa z})^2}\right). \tag{2.67}$$

Since both in the numerator as well as in the denominator a $e^{-\kappa z}$ term is present, an anti-derivative can be found

$$2(\cosh(\phi(z))-1) = \frac{-4}{\kappa}\frac{d}{dz}\left(\frac{1}{(1-\gamma e^{-\kappa z})}-\frac{1}{(1+\gamma e^{-\kappa z})}+C_1\right) = \frac{-8}{\kappa}\frac{d}{dz}\left(1+\frac{\gamma^2 e^{-2\kappa z}}{1-\gamma^2 e^{-2\kappa z}}+C_1\right). \tag{2.68}$$

With C_1 an arbitrary constant. Again there is an $e^{-2\kappa z}$ both in the numerator as well as the denominator so an anti-derivative can be found

$$2(\cosh(\phi(z))-1) = \frac{-8}{\kappa^2}\frac{d^2}{dz^2}\left(z+\frac{1}{2}\ln\left(1-\gamma^2 e^{-2\kappa z}\right)+C_1 z+C_2\right). \tag{2.69}$$

This expression can now be substituted into equation (2.66)

$$\eta\frac{d^2u_x(z)}{dz^2} = \frac{-8k_{\mathrm{B}}T}{\kappa^2}\frac{d\rho_b(x)}{dx}\frac{d^2}{dz^2}\left(z+\frac{1}{2}\ln\left(1-\gamma^2 e^{-2\kappa z}\right)+C_1 z+C_2\right). \tag{2.70}$$

The first constant is found realizing that the velocity derivatives in the middle of the channel vanish because the electric potential from the EDL vanishes, this gives $C_1 = -1$. The second constant is obtained from the no slip boundary condition: $u_x(0) = 0$ and yields $C_2 = \ln(1-\gamma^2)$. The final result for the fluid velocity in the channel is then

$$u_x(z) = -\frac{4k_{\mathrm{B}}T}{\eta\kappa^2}\frac{d\rho_b(x)}{dx}\left(\ln\left(\frac{1-\gamma^2 e^{-2\kappa z}}{1-\gamma^2}\right)\right) = -\frac{k_{\mathrm{B}}T}{2\eta\pi\lambda_{\mathrm{B}}\rho_b(x)}\frac{d\rho_b(x)}{dx}\left(\ln\left(\frac{1-\gamma^2 e^{-2\kappa z}}{1-\gamma^2}\right)\right). \tag{2.71}$$

Where in the last equality the definition of the Debye length (equation (2.31)) has been used. Note that it is assumed the difference in salt concentration between the reservoirs is small enough that the Debye length stays constant. Now even though the fluid velocity is induced by the pressure gradient along the inhomogeneous EDL, that is induced by the interaction between the salt concentration gradient and the electric potential from the surface charge, it is not only non-zero in the Debye-layer where the electric potential is non-zero. The resulting pressure gradient in the x-direction is present along the whole cross-section of the channel and thus induces a fluid flow across the whole channel!

Now outside the EDL the fluid velocity is (remember that the expression for the EDL potential has been derived for a single charged surface at $z = 0$, so z to ∞ here means z to $H/2$)

$$u_{DO} = -\frac{k_{\mathrm{B}}T}{2\eta\pi\lambda_{\mathrm{B}}\rho_b}\frac{d\rho_b(x)}{dx}\ln\left(1-\gamma^2\right) = -\frac{1}{2\eta\pi\lambda_{\mathrm{B}}}\frac{d\mu(x)}{dx}\ln\left(1-\gamma^2\right). \tag{2.72}$$

Where $(1/\rho_b(x))(d\rho_b(x)/dx)$ has been reduced to $d\mu(x)/dx$ using the relation from equation (2.43) The fluid volume flux in the x-direction per unit distance in the y-direction is now given by

$$Q_u = 2\int_0^{H/2} dz u_x(z) = HU_{DO} - \frac{k_\mathrm{B}T}{\eta\pi\lambda_\mathrm{B}}\frac{d\mu(x)}{dx}\int_0^{H/2} dz \ln\left(1-\gamma^2 e^{2\kappa z}\right). \tag{2.73}$$

This last integral is a special integral called a polylogarithmic function. Which can be written as an infinite sum of elementary functions[11]

$$Q_u = HU_{DO} + \frac{k_\mathrm{B}T}{\eta\pi\lambda_\mathrm{B}\kappa}\frac{d\mu(x)}{dx}\frac{\mathrm{Li}_2(\gamma^2)}{2}. \tag{2.74}$$

What this polylogarithmic function is exactly, is not of great importance here. The crux is that the integral has a general linear response relation. Thus in that sense an analytic solution has been found.

The different currents can also be found, starting with the advective charge flux in the x-direction per unit length in the y-direction from equation (2.48)

$$I_\mathrm{adv} = -2\epsilon_0\epsilon\int_0^{H/2} dz u_x(z)\frac{d^2\psi(z)}{dz^2}, \tag{2.75}$$

where the Poisson-Boltzmann equation (2.22) has been used to eliminate the ionic charge density. Now this equation can be integrated twice using partial integration to yield

$$\begin{aligned} I_\mathrm{adv} &= 2\epsilon_0\epsilon u_x(0)\frac{d\psi(0)}{dz} + 2\epsilon_0\epsilon\int_0^{H/2} dz\frac{d\psi(z)}{dz}\frac{du_x(z)}{dz} \\ &= -2\epsilon_0\epsilon\psi(0)\frac{du_x(0)}{dz} - 2\epsilon_0\epsilon\int_0^{H/2} dz\psi(z)\frac{d^2u_x(z)}{dz} \\ &= -2\epsilon_0\epsilon\int_0^{H/2} dz(\psi(z)-\psi(0))\frac{d^2u_x(z)}{dz^2}, \end{aligned} \tag{2.76}$$

where $d\psi(H/2)/dz = 0$ and $du_x(H/2)/dz = 0$ have been used and the first term in the first line has been ignored because of the no slip boundary condition $u_x(0) = 0$. Now using equation (2.66) to eliminate the fluid velocity

$$\begin{aligned} I_\mathrm{adv} &= -2\epsilon_0\epsilon\frac{2(k_\mathrm{B}T)^2}{\eta e}\frac{d\rho_b(x)}{dx}\int_0^{H/2} dz(\phi(z)-\phi(0))(\cosh(\phi(z))-1) \\ &= -\frac{k_\mathrm{B}e}{\pi\eta\lambda_\mathrm{B}}\frac{d\rho_b(x)}{dx}\int_0^{H/2} dz(\phi(z)-\phi(0))(\cosh(\phi(z))-1) \\ &= -4\frac{k_\mathrm{B}e}{\pi\eta\lambda_\mathrm{B}\kappa}\frac{d\rho_b(x)}{dx}\Big(2\sinh(\phi(0)/2)-\phi(0)\Big) \\ &= \frac{4k_\mathrm{B}Te}{8\pi^2\eta\lambda_\mathrm{B}^2\rho_b(x)}\frac{d\rho_b(x)}{dx}\Big(2\sinh(\phi(0)/2)-\phi(0)\Big) \\ &= \frac{e}{2\pi^2\eta\lambda_B^2}\frac{d\mu(x)}{dx}\Big(2\sinh(\phi(0)/2)-\phi(0)\Big), \end{aligned} \tag{2.77}$$

where again the definitions of the Debye (2.31) and Bjerrum length (2.30) have been used to further simplify the expression.

The diffusive charge flux contribution in the x-direction is given by the first term from the Nerns-Planck equation (2.46) with again $D_+ = D_- = D =$ constant

$$I_{\text{diff}} = 2D \int_0^{H/2} dz \frac{\partial}{\partial x}(\rho_+(x,z) - \rho_-(x,z)), \tag{2.78}$$

using the Boltzmann distribution (2.23) this can be reduced to

$$I_{\text{diff}} = -4D \frac{\partial \rho_b(x)}{\partial x} \int_0^{H/2} dz \sinh(\phi(z)), \tag{2.79}$$

where it is assumed that the potential only depends on the z-coordinate and the bulk ion concentration only depends on the x-coordinate. Again like equation (2.60), since the surface charge must be entirely screened by oppositely charged ions, the integral reduces to

$$I_{\text{diff}} = \frac{2D}{\rho_b(x)} \frac{\partial \rho_b(x)}{\partial x} z_s \rho_s = 2D\beta \frac{\partial \mu(x)}{\partial x} z_s \rho_s. \tag{2.80}$$

The total current is now given by

$$I = I_{\text{adv}} + I_{\text{diff}} = \frac{e}{2\pi^2 \eta \lambda_B^2} \frac{d\mu(x)}{dx} \Big(2\sinh(\phi(0)/2) - \phi(0) \Big) + 2D\beta \frac{\partial \mu(x)}{\partial x} z_s \rho_s. \tag{2.81}$$

2.8 Linear response

So far it has been demonstrated that pressure gradient in the electric double layer configuration does not only induce a fluid volume flux but also a current. In the same way an external electric field does not only induce a current but also a fluid volume flux and furthermore a chemical potential gradient induces a volume flux as well as a charge flux. Note that the conjugated flux to the chemical potential gradient is a salt flux that is not considered here. Also other fluxes, e.g. a heat flux, are the result of the considered driving forces but are not considered here. The induced fluxes are linear in their driving forces, for small driving forces. All the considered results can be combined into a single matrix vector equation:

$$\begin{pmatrix} Q_u \\ I \end{pmatrix} = \begin{pmatrix} L_{11} & L_{12} & L_{13} \\ L_{21} & L_{22} & L_{23} \end{pmatrix} \begin{pmatrix} -\frac{dp}{dx} \\ E_x \\ \frac{d\mu(x)}{dx} \end{pmatrix}. \tag{2.82}$$

Where $\boldsymbol{L}$ is also called the Onsager matrix. Equation (2.19) yields the first Onsager coefficient:

$$L_{11} = \frac{1}{12} \frac{1}{\eta} H^3, \tag{2.83}$$

equation (2.49) yields:

$$L_{21} = -\frac{\epsilon_0 \epsilon H}{\eta} \psi(0), \tag{2.84}$$

equation (2.55) yields:

$$L_{12} = -\frac{\epsilon_0 \epsilon H}{\eta}\psi(0), \tag{2.85}$$

equation (2.61) yields:

$$L_{22} = \frac{8\beta^2 e^2 \epsilon_0^2 \epsilon^2 \kappa}{\eta}(\cosh(\phi(0)/2) - 1) - 2e^2\beta D z_s \rho_s, \tag{2.86}$$

equation (2.74) yields:

$$L_{13} = -\frac{H}{2\eta\pi\lambda_{\mathrm{B}}}\ln\left(1-\gamma^2\right) + \frac{k_{\mathrm{B}}T}{\eta\pi\lambda_{\mathrm{B}}\kappa}\frac{\mathrm{Li}_2(\gamma^2)}{2}, \tag{2.87}$$

and finally, equation (2.81) yields

$$L_{23} = \frac{e}{2\pi^2\eta\lambda_B^2}\Big(2\sinh(\phi(0)/2) - \phi(0)\Big) + 2D\beta z_s\rho_s \tag{2.88}$$

Note the symmetry $L_{21} = L_{12}$, which is always true for the Onsager matrix. Also keep in mind that these relations have been derived assuming non-overlapping EDL's, i.e. $z < \kappa^{-1} \ll H$. The theory can be easily extended to overlapping double layers, but for simplicity non-overlapping double layers will be considered for now.

To recapitulate: due to the presence of the EDL, a pressure gradient induces not only a fluid volume flux, but also an electric current; an external electric field induces not only an electric current, but also a fluid volume flux and a salt concentration gradient also induces both a fluid volume flux and an electric current. Note that also other fluxes are induced that are not considered here such as a salt flux and a heat flux. These fluxes are all, for small enough driving forces, linear in their driving force.

3 Numerical model

The theory derived in section 2 for transport of fluids and charges between two surfaces driven by an external electric field or pressure gradient, can now be used to model the fluid and charge flow going through nanopores. To numerically model the equations derived in the previous section the computer program *COMSOL Multiphysics 5.2* (from now on just *COMSOL*) is used. Firstly, to test the validity of the numerical model, the linear response relations from the Onsager matrix (2.82) are considered, such that it is known in which parameter regimes the outlined theory holds.

3.1 Geometry and mesh

The geometry used to test the linear response relations can be seen in figure 3.1a. The geometry is chosen such that the length of the channel is much larger than the width, such that the reservoirs are large enough that they can be seen as baths with a fluid volume and charge volume that changes negligibly small compared to the changes in the channel and

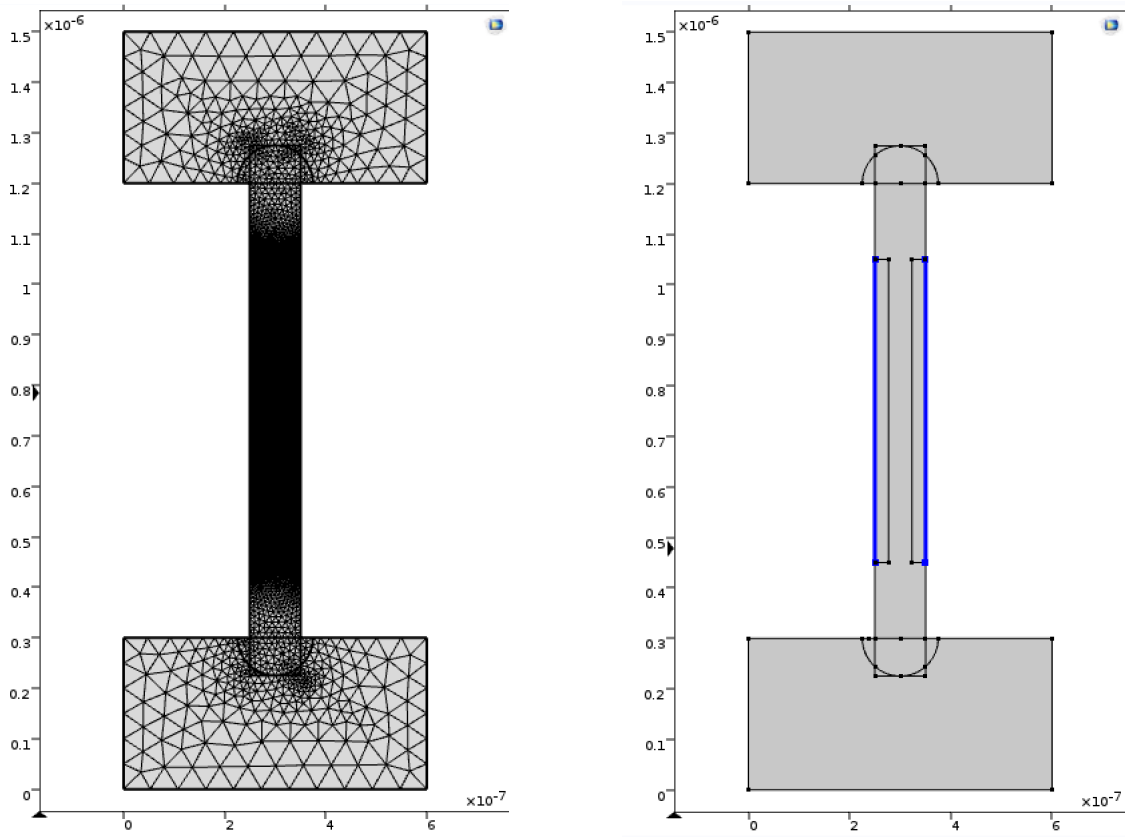

(a) Mesh

(b) Surface charge on highlighted (blue) surface

Figure 3.1: Geometry of the model in *COMSOL*, with maximum reservoir mesh size: $5.6 \cdot 10^{-8}$m, maximum middle of the channel mesh size: $1.5 \cdot 10^{-8}$m, maximum Debye layer mesh size: $2.0 \cdot 10^{-9}$m and surface charge density along the blue surface's: $\rho_s = 1.6022 \cdot 10^{-3}\text{C/m}^2$. All other paramters are in table 1 in section 4. The vertical axis is referred to as the x-axis and the horizontal axis as the z-axis. Both large regions that are connected to each other are referred to as the reservoirs and the connection between them is referred to as the channel.

such that the Debye length is a factor 10 smaller than the channel width such that non-overlapping EDL's are considered. The triangular shaped area's are called the mesh. A mesh is used to discretize the area in which the differential equations have to be solved. In general it can be seen in a way that *COMSOL* solves the equations to be solved for every mesh point (triangle) and gives the desired physical variable as a polynomial over that mesh point. Once there are enough mesh points in the system the solutions will closely resemble the continuous analytical solutions describing the same problem. The geometry is chosen in a way that there is a large enough bath on both sides of the channel such that all the variables decay to bulk values. This is why in the reservoir it is not needed to have a high resolution mesh because all the variables stay close to constant here. In the same way the mesh inside the channel has to be of a resolution that makes sure the behaviour of the system inside the Debye layer, where the most dramatic changes (such as potential drop off) happen, is fully captured in the solutions. A mesh with a resolution that is too high will take too much computation time. So it is important to find a mesh that is accurate enough to capture the behaviour of the system but not too small that it takes too much time to solve the equations. In order to do this inside the Debye layer, a mesh is chosen of a factor 10 smaller than the length of the Debye layer. If the solutions appear to be continuous, there is no reason to change the mesh resolution. Once discontinuities start appearing in the solutions, the mesh resolution should be taken into consideration again. Also note that near the boundaries of the channel and the reservoir the mesh resolution is higher as well. This is because near the inlet and outlet entrance effects give complex physics. This is also why at first only an EDL in the middle of the channel is considered, to not have to deal with these boundary effects, see figure 3.1b.

3.2 Implementing physics into *COMSOL*

COMSOL is now ready to solve the differential equations describing electrokinetic flow, i.e. the theory from the previous section can be tested in the geometry outlined above, i.e. *COMSOL* can now solve the Poisson-Nernst-Planck-Stokes equations (2.22), (2.46) and (2.13). The fluid flow that is described by the steady state Navier-Stokes equation (2.12) and the continuity equation are solved by *COMSOL* using the module *Creeping Flow* (CF). For every specific case, boundary conditions can be implemented. The fluid and transport properties used, can be seen in table 1 in section 4. Note that from now on the channel height H from the theory section has been replaced by the channel width W. The charged particle flow that is described by the Nernst-Planck equation (2.46) is solved by *COMSOL* using the module *Transport of Diluted Species* (TDS). The EDL described in the previous chapter can be modelled into *COMSOL* using several ways, the way that is used here is by adding a surface charge density ρ_s to the surface in the channel (not along the whole channel for reasons just discussed) using the *Electrostatics* (ES) module in *COMSOL*, see figure 3.1b. Also for the *Electrostatics* module, the boundary conditions can be changed for every specific case and will be discussed below.

These three modules discussed are the only modules needed to reproduce the linear response relations. They are coupled in the following way: The external electric field (from the ES module) interaction with the charge density from the ions (from the TDS module) can be added as a volume force term to the Navier-Stokes equation (in the CF module) as:

$e(\rho_+ - \rho_-)E_x$ and the TDS module is set to solve the Nernst-Planck equations using the fluid velocity from the CF module and the electric potential from the ES module. All parameters are now set and yield a Debye Length of $\kappa^{-1} = 9.6 \cdot 10^{-9}$m. This means the channel is more than 10 Debye lengths wide, which should ensure there is no overlaying EDL effect.

3.2.1 External pressure gradient

By applying an external pressure gradient along the model setup that is now established, the first two linear response relations can be considered by calculating the fluid volume flux in the x-direction per unit length in the y-direction and the streaming current, i.e. the net charge flux in the x-direction per unit length in the y-direction. An external pressure gradient is applied in the CF module by setting an inlet of pressure $P = P_0$ at the top horizontal surface and an outlet at the bottom horizontal surface which is set to $P = 0$. To keep the ion concentration constant in the reservoirs an inflow from both the outer most horizontal surfaces of $\rho_+ = \rho_- = 1\text{mol/m}^3$ is implemented in the TDS module. Furthermore the electric potential at the surfaces is set to zero everywhere but at the surface of the EDL since there is no external electric field in this case and such that a closed electric circuit is considered. For every imposed pressure gradient both the fluid volume flux and the net charge flux can be derived from *COMSOL*.

3.2.2 External electric field

By applying an external electric field to the model, the second two linear response relations can again be reproduced by calculating the resulting fluid volume flux and net charge flux in the x-direction per unit distance in the y-direction. An external electric field is applied in the ES module by setting an electric potential $V = V_0$ at the top horizontal surface and an electric potential of $V = 0$ at the bottom horizontal surface (V is always zero here). The electric potential has initial value 0 at all boundaries. Both horizontal surface pressure inlets are kept constant at $P = P_0$ in the CF module as well as both ion inflows from both the outer most horizontal surfaces of $\rho_+ = \rho_- = 1\text{mol/m}^3$ to keep the ion concentration constant in the reservoirs. Now a range of electric fields can be imposed and again both the fluid volume flux and the net charge flux can be derived from *COMSOL*.

3.2.3 External chemical potential gradient

The last tested driving force is the external chemical potential gradient, to again verify the linear response from the fluid volume flux and the net charge flux in the x-direction per unit length in the y-direction. The chemical potential gradient is applied by setting an inflow salt concentration of ρ_{in} at the top horizontal surface that is greater than the inflow salt concentration ρ at the bottom horizontal surface. Furthermore, all other surfaces have imposed no flux boundary conditions, both horizontal surface pressure inlets are kept constant at $P = P_0$ and the electric potential is set to zero everywhere except at the regions with surface charge (at the EDL). Now also a double layer that extends all the way around the corner of the inlet will be considered since this might be a more realistic configuration. Although it is not yet fully known where along the surface the EDL extends in such nanoscale membranes, it seems more realistic to have it extend around the corner of the inlet [8]. Both cases with

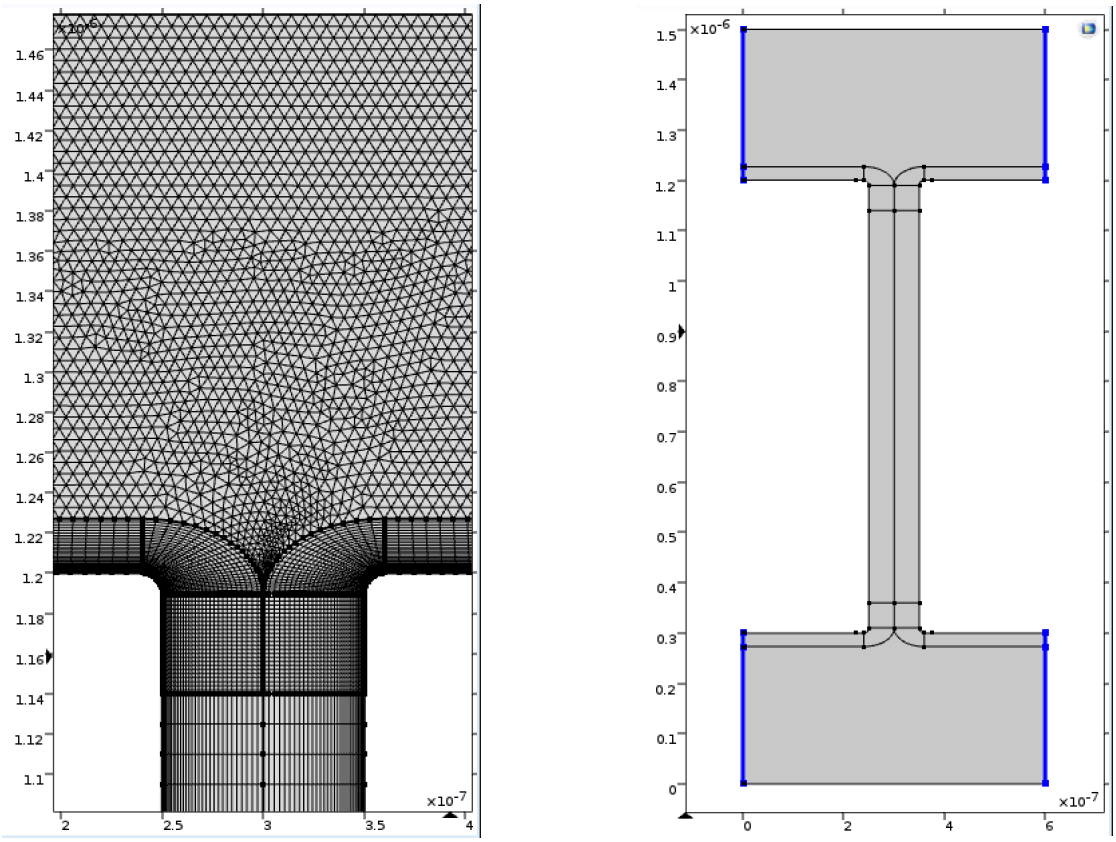

(a) Mesh

(b) Periodic boundary conditions

Figure 3.2: Geometry of a the finer mesh model in *COMSOL*, with maximum reservoir mesh size: $7.0 \cdot 10^{-9}$m, maximum mesh size at the inlet: $2.0 \cdot 10^{-9}$m, maximum mesh size in the z-direction in the middle of the channel of: $3.0 \cdot 10^{-9}$m, with a finer mesh size at the Debye layer of: $1.0 \cdot 10^{-9}$m. The blue surfaces are imposed to periodic boundary conditions. Again all other paramters are given by table 1 in section 4. The vertical axis is referred to as the x-axis and the horizontal axis as the z-axis

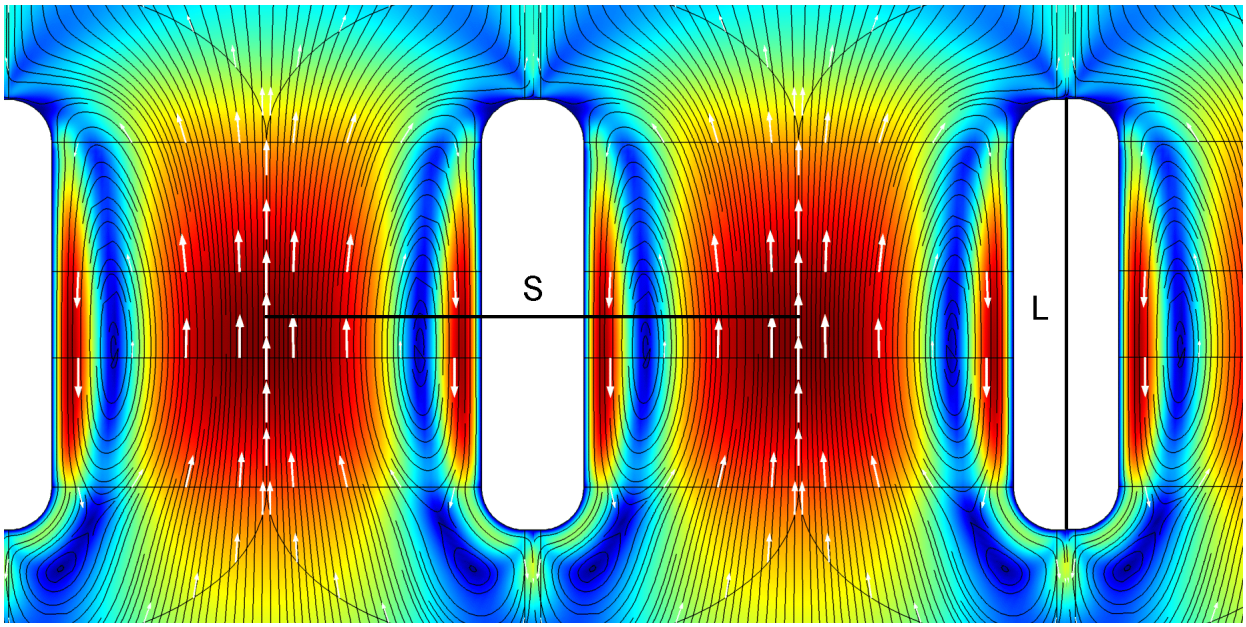

Figure 3.3: Schematic display of an chain of channels with distance S between them and of length L. Here $S = 1.25W$ with W the width of the channel. The horizontal direction is the z-direction, the vertical direction is the x-direction, leaving the y-direction going out of the paper.

and without an extended surface charge are tested to see if this makes any difference in the linear response relation. In order to do this, the geometry has to be altered such that a surface charge can be smoothly extended around the corner. Also entrance effects are now more important since the double layer is now also present at the entrance, this means the mesh resolution must be higher than before. In figure 3.2a the new mesh can be seen. Now a range of inlet concentrations, ρ_{in}, can be imposed and both the volume flux and the net charge flux can be derived from $COMSOL$

3.2.4 Periodic boundary conditions

Finally, when all linear response relations have been considered, such that the regime in which the fluxes react linearly to the driving forces. Periodic boundary conditions can be implemented to simulate an infinitely long chain of nanopores with the goal of finding an optimal porosity, see figure 3.3. Periodic boundary conditions are implemented by adding periodic boundary conditions to all three modules for the regions highlighted in figure 3.2b. For the CF module this means pressure at the left boundary must be equal to the pressure at the right boundary, as well as the fluid velocity must be equal on both sides (velocity, so magnitude and direction). For the TDS module this means the salt concentration must be equal on both sides and for the ES module this means the electric potential must be equal on both sides. With periodic boundary conditions implemented any fluid flow coming in from one side, must have an exactly equal fluid flow going out from the other side. Now the fluxes for different distances between channels can be investigated.

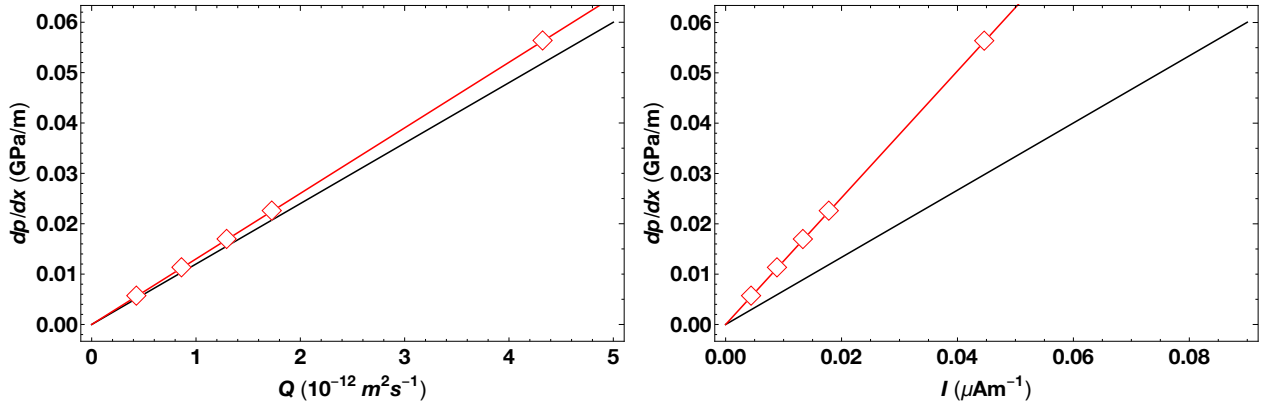

(a) (b)

Figure 4.1: The induced fluid volume flux (a) and electric current (b) (red dots) from the imposed pressure gradient to the nanopore model in *COMSOL* of $P_0 = 0.05$, 0.1, 0.15, 0.2, 0.25 and 0.5 atm, plotted with the analytic relation between the pressure gradient and the volume flux (black line): $\frac{dp}{dx} = \frac{12\eta Q}{W^3}$ (equation 2.19) and with the analytic relation between the pressure gradient and the electric current: $\frac{dp}{dx} = \frac{I\eta}{\epsilon 0 \epsilon W \psi(0)}$ (equation 2.49).

4 Results

In this section, first the linear response relations between the considered driving forces and their induced fluxes are considered after which the length scales, length of the channel L and distance between channels S are varied with the salt concentration gradient as driving force. All quantities are plotted as absolute values for aesthetic reasons, such that they are plotted in the first quadrant, from the Onsager matrix (2.82) it should be obvious what the sign of the different quantities is. In table 1 all parameter values are listed.
Some of the linear response relations will not be fully reproduced unfortunately, most likely due to (small) calculational errors in the theory section, which have not all been found yet. This does not mean that the data given out by *COMSOL* should be seen as false. *COMSOL* solves the PNPS equation to derive the fluid and (charged) particle flow, just like in the theory section the different linear response relations have been derived from the PNPS equations. Since it is known that the PNPS equation are correct, the results in COMSOL, coming from solving just these equations, do not have to be seen as uncorrect. These results are numeric solutions to the PNPS equations that, despite the good efforts in this thesis, have not yet been fully derived theoretically.

4.1 Linear response relations

4.1.1 External pressure gradient

In figure 4.1a it can be seen that the first linear response relation between the fluid volume flux and external pressure gradient has been nearly reproduced. The fluid flux is a factor 7.8% smaller than the analytic solution. This effect can be attributed to entrance effects because linear response theory does not take these entrance effects into account.

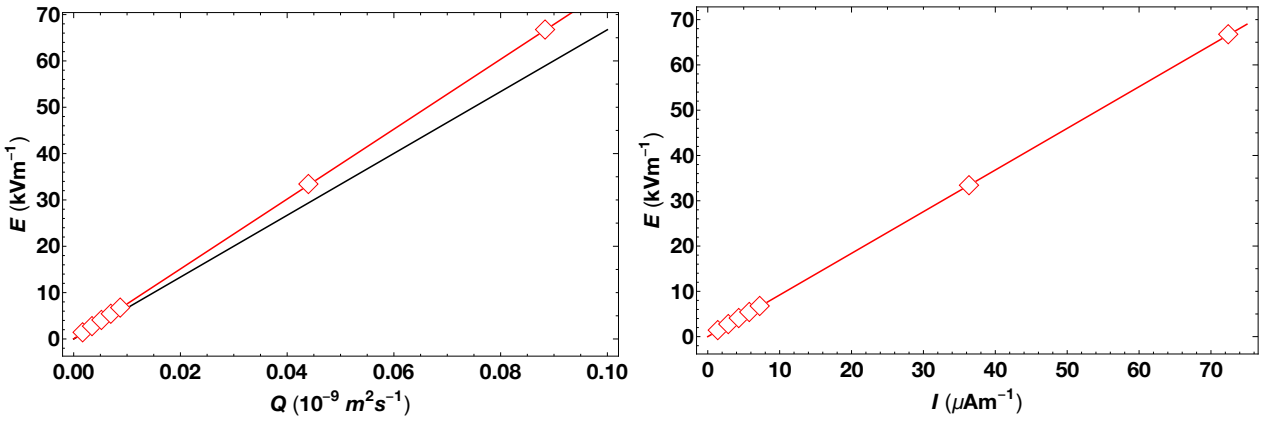

(a) (b)

Figure 4.2: The induced fluid volume flux (a) and electric current (b) (red) from the imposed electric field to the nanopore model in *COMSOL* of $V_0 = 0.002$, 0.004, 0.006, 0.008, 0.01, 0.05 and 0.1 V, plotted with the analytic relation between the electric field and the volume flux (black): $E_x = \frac{Q_u \eta}{\epsilon 0 \epsilon W \psi(0)}$ (equation 2.55) but without the analytic relation between the pressure gradient (equation 2.61).

In figure 4.1b it can be seen that the linear response relation between the streaming current and external pressure gradient has not been perfectly reproduced but misses out by a factor of two. Unfortunately this factor has not been found, most probable is that it is a data processing error or a theory error where, e.g. only half the channel has been considered. As obvious as this seems, the error has not been found. The electric current does respond linearly to the pressure gradient though, so, qualitatively, linear response holds for the regime considered.

4.1.2 External electric field

In figure 4.2a it can be seen that the first linear response relation between the fluid volume flux and the external electric field has been nearly reproduced. The fluid volume flux is now a factor 11.5% smaller than the analytic solution. This effect can again be attributed to entrance effects.
In figure 4.2b it can be seen that the analytic solution of the electric current driven by an external electric field is not plotted at all, this is because the discrepancy between the data and the analytic solution form the theory is an order of magnitude. This must be due to an error in the derivation of the L_{22} Onsager coefficient, but this error unfortunately has not been found for now. Again the electric current does respond linearly to the electric field, so in the regime considered linear response is valid. It only cannot be reproduced exactly up to the right prefactor.

4.1.3 External chemical potential gradient

In figure 4.3 both the fluid flux and the electric current for channel lengths $L = 0.1\mu$m and $L = 0.9\mu$m have been plotted against the chemical potential gradient for a surface charge

extending all the way around the corner of the in- and outlet and for a surface charge present only in the channel. The linear relations plotted are fits over the fist data points at low salt concentration gradients, namely from $\rho_{in} = 1.1$ to $\rho_{out} = 1.3$. It can be seen that the linear relation between the fluid flux and the salt concentration gradient does not hold anymore for $\rho_{in}/\rho_{out} \approx 1.5$ for both $L = 0.1\mu$m and $L = 0.9\mu$m. When investigating the porosity of the membrane, it should be kept in mind that the linear response region for the salt concentration gradient is in this range. Note that the term porosity in this thesis is used to conveniently consider both the channel length and distance between channels at them same time. Nothing else is done with this term and the reader can just read porosity as: distance between channels and the length of the channel. It can also be seen that for $L = 0.1\mu$m the fluid flux for the surface charge extending all the way around the corner has a slope in the linear response region of approximately four times as high as the slope of the fluid for the surface charge only in the channel and the electric current has a slope in the linear response region of approximately 1.75 times as high as the slope of the fluid for the surface charge only in the channel. For $L = 0.9\mu$m the electric current has a significant discrepancy between the fully charged surface and the channel charged surface. The electric current for the fully charged surface follows linear response throughout the whole range, while the electric current from the system with only the surface in the channel charged fails to follow linear response after $\rho_{in}/\rho_{out} \approx 5$. For $L = 0.1\mu$m the electric current fails to follow linear response after approximately $\rho_{in}/\rho_{out} \approx 2$
For the fluid flux and the electric current for both the surface charge extending around the corner and the surface charge only present in the channel, the linear response relations hold for all small salt concentration gradients up until $\rho_{in}/\rho_{out} \approx 1.5$. After that the fluid fluxes and the electric currents for $L = 0.9\mu$m and the electric current for only a channel charged surface with channel length $L = 0.9\mu$m response to the salt concentration gradient start to break down respectively.
Unfortunately again the analytic solutions have not been plotted against the data from $COMSOL$ here. The derivation done in the theory section was lengthy and thus prone to errors, so for now the analytic solution does not match the data yet correctly. Again though, the regime in which the system follows linear response has been found.

4.2 Optimal porosity

The goal is now to find an optimal porosity for a nanoscale membrane to maximize the fluid volume flux and the net charge flux, because in the end this can be used to find the maximum generated power. Using periodic boundary conditions, an infinitely long chain of channels can be simulated, see figure 3.3, of which the channel distance S and channel length L can be modified. These variations of the geometry are done for a system with a chemical potential gradient, since this driving forced is used for RED to generate blue energy and is most present in literature. In the previous section the linear response regime for the salt concentration gradient has been found. This has led to a choice of salinity gradient of $\rho_{in}/\rho_{out} = 1.2$ as the driving force of the system. Note that the linear response regime does not have to be the same for systems with other geometries, it has been shown in figure 4.3 that for both channels of small and large lengths, there is a regime in which the fluxes react linearly to a

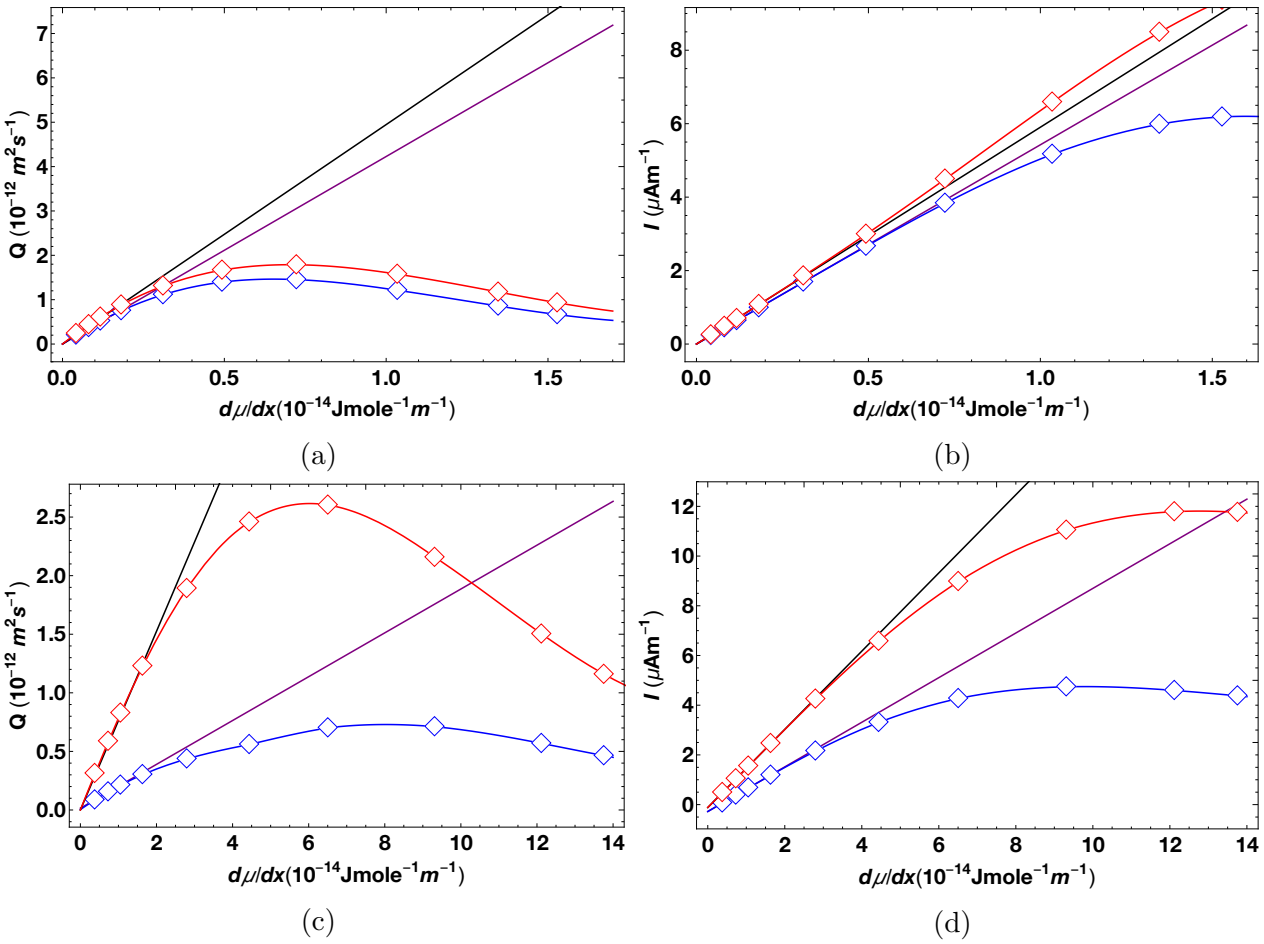

Figure 4.3: The fluid volume flux and electric current for $L = 0.9\mu$m (a) and (b) and $L = 0.1\mu$m (c) and (d) resepectively in the x-direction per unit lentgh in the y-direction for a surface charge extending all the way around the corner (Red) of the inlet and for a surface charge not extended around the corner (Blue) plotted with the linear response found for small salt concentration gradients, namely ρ_{in} =[1;1.3]mol/m^3, with the black line corresponding to the surface charge all the way around the corner (Red) and the purple line corresponding to the surface charge not around the corner of the inlet (Blue). The chemical potential gradient range corresponds to a range $\rho_{in}/\rho_{out} = [1.1; 30]$.

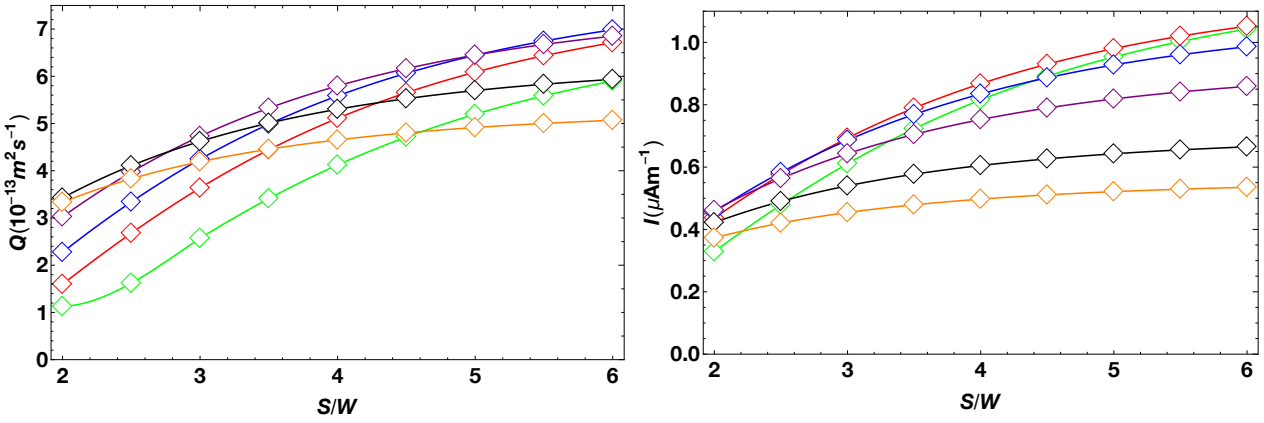

(a) Fluid flux

(b) Electric current

Figure 4.4: The fluid volume flux (a) and electric current (b) in the x-direction per unit length in the y-direction for different channeldensities (the distance between channels is given as a multiple of the channel width W) for channel lengths: $L = 0.1\mu$m, green; $L = 0.15\mu$m, red; $L = 0.20\mu$m, blue; $L = 0.3\mu$m, purple; $L = 0.5\mu$m, black. With the surface charge extending all the way around the corner of the inlet.

salt concentration gradient change. For smaller distance between channels this has not yet been shown and it is likely that linear response breakdown due to an increase in entrance effects. It is still interesting to pursue such geometries though and when finding interesting results it can always be checked when they have been found in linear response theory or not. In figure 4.4 the fluid volume flux and in figure 4.4b the electric current through a nanopore with geometry as in figure 3.2b in the x-direction per unit length in the y-direction for different distances between channels for different channel lengths L are plotted.

5 Discussion

This discussion will primarily focus on the difference in porosity that has been investigated, since the linear response relations are expected outcomes and therefore will not lead to new insight regarding the research questions outlined in the introduction. Though the theory has not been able to exactly verify the model simulations, this is merely a case of thoroughly going over the derivations until validity can be assured. This is not the case just yet and since [8] has shown the linear response theory from the Onsager matrix 2.82 should verify the considered systems up to errors coming, e.g. from entrance effects and not up to orders of magnitude. The investigation of the different driving forces versus the flux relations are thus used as a guideline in which regimes the linear response theory holds and for which in principle analytic solutions can be found.

In figure 4.4 it can be seen that as the distance between channels grows, the fluid volume flux through the channel increases. This means that the smaller the distance between channels, the more the in- and outgoing flow is interfering with the in- and outgoing flow from channels next to it. The greater the distance between the channels the more negligible this effect becomes and thus eventually the fluid flux stays the same when increasing the distance

Quantity	Symbol	Value	Unit
Inlet salt concentration upper reservoir	$\rho^1_- = \rho^1_+$	1.20	mol/m^3
Inlet salt concentration lower reservoir	$\rho^2_- = \rho^2_+$	1.20	mol/m^3
Surface charge	ρ_s	$1.60 \cdot 10^{-4}$	C/m^2
Upper boundary electric potential	V_0	0	V
Relative permittivity	ϵ	80.0	1
Temperature	T	293.15	K
Bjerrum length	λ_B	$7.13 \cdot 10^{-10}$	m
Debye length ϵ	κ^{-1}	$9.63 \cdot 10^{-9}$	1
Mass density	ρ	1000	kg/m^3
Dynamic viscosity	η	$10 \cdot 10^{-4}$	pa·s
Diffusion coefficient	$D_+ = D_- = D$	$1 \cdot 10^{-9}$	m$^2/s$
Charge valancy	$z_+ = -z_-$	1	1
Channel width	W	$1 \cdot 10^{-7}$	m
Channel Length	L	$0.9 \cdot 10^{-6}$	m

Table 1: Relevant parameter values of water that are used in $COMSOL$ for the single channel model, so the simulations without periodic boundary conditions.

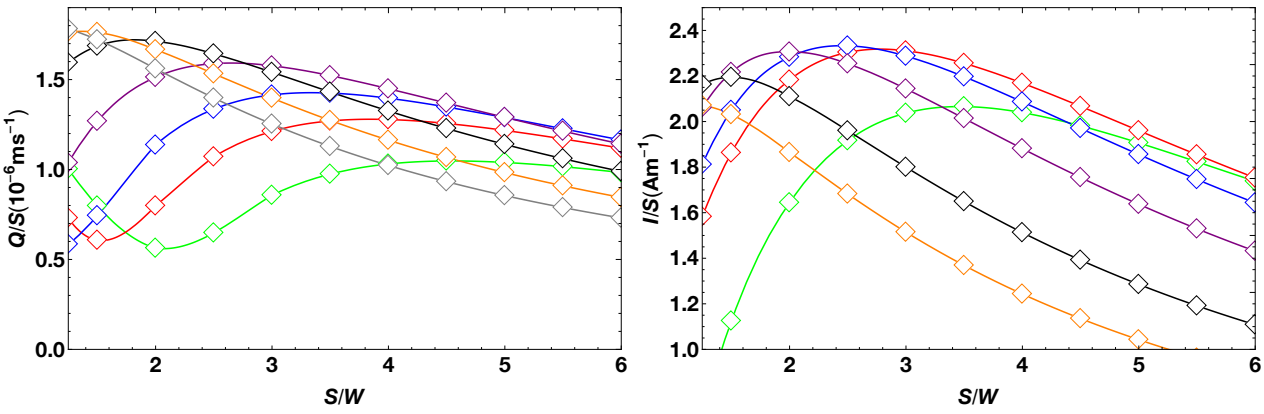

(a) Fluid flux

(b) Electric current

Figure 5.1: The fluid volume flux (a) and electric current (b) in the x-direction per unit length in the y-direction divided by the distance between the channels for different channeldensities (the distance between channels is given as a multiple of the channel width W) for channel lengths: $L = 0.1\mu$m, green; $L = 0.15\mu$m, red; $L = 0.20\mu$m, blue; $L = 0.3\mu$m, purple; $L = 0.5\mu$m, black; $L = 0.7\mu$m, orange; and for the fluid flux $L = 0.9\mu$m has been added in gray. The surface charge extends all the way around the corner of the inlet.

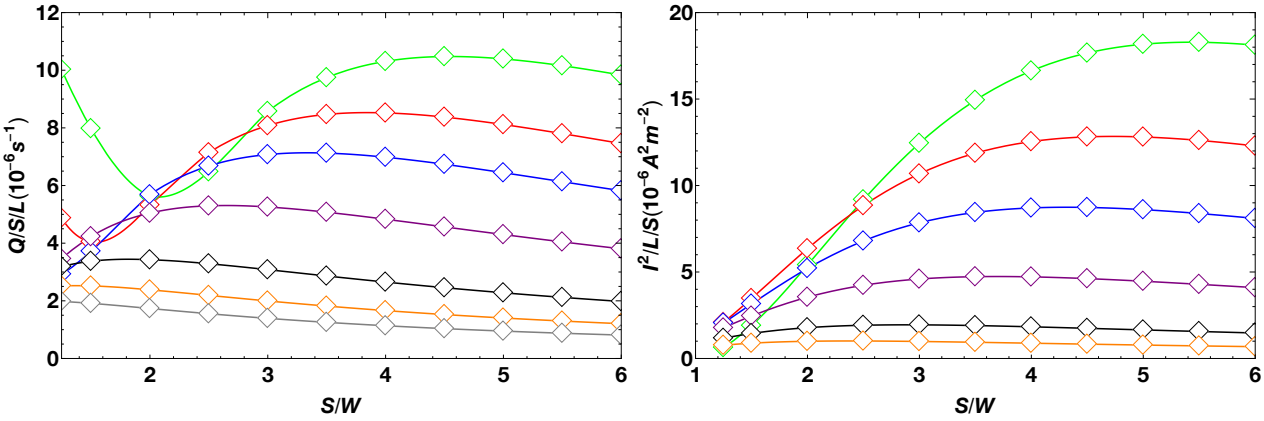

(a) Fluid flux (b) Electric current

Figure 5.2: The fluid flux (a)in the x-direction per unit length in the y-direction squared and divided by the distance between the channels and the length of the channels and electric current (b) in the x-direction per unit length in the y-direction squared and divided by the distance between the channels and the length of the channels, which goes the same as the generated power of the chain of channels but differs by a multiplicative factor, given for different channeldensities (the distance between channels is given as a multiple of the channel width W) for channel lengths: $L = 0.1\mu$m, green; $L = 0.15\mu$m, red; $L = 0.20\mu$m, blue; $L = 0.3\mu$m, purple; $L = 0.5\mu$m, black; and $L = 0.7\mu$m in black. The surface charge extends all the way around the corner of the inlet.

between channels. This corresponds to the fluid flux going asymptotically to a max value for a large distance between channels. At large distances there is no interference anymore between the channels next to each other, so increasing the distance between the channels does not make a difference anymore for the fluid flux going through the channel. At small distances between the channels the effect of decreasing interference makes a significant difference, but becoming less and less important when increasing the distance between the channels. This explains the exact shape of the plots from 4.4. It is interesting to see that the flux for maximum channel distance ($6W$) is initially increasing as L increases but after $L = 0.20\mu$m is decreasing again. A larger channel length L means a smaller salt concentration gradient, so it is to be expected that the fluid flux decreases when increasing the channel length. For small enough channel lengths this is not the case anymore though! Again interference from neighbouring channels must block the fluid flux when the channel length is getting too small. For the channel distance ($2W$) it can be seen that fluid flux is only increasing when increasing the channel length. Apparently the relief from the interference effects still outweighs the decrease in salt concentration gradient. For all distances between channels effects like this can be seen. The larger the distance between channels, the smaller the channel length at which the switch from increasing flux to decreasing flux begins. In figure 4.4 this turnaround point can be precisely found for every distance between channels. For the interval $S/W = [5, 6]$ the turnaround point is between $L = 0.2\mu$m and $L = 0.3\mu$m and for $S/W = [3, 5]$ the turnaround point is between $L = 0.3\mu$m and $L = 0.5\mu$m.

A natural conclusion from these observations would be that maximum flux per unit surface, or in this case per unit length since essentially a 1-dimensional chain of channels is considered, will not necessarily arise at minimal channel length, where the salt concentration gradient is maximum and at minimal distance between channels, where the number of channels per unit length is maximum. Interference effects at the in- and outlets lead to suppression of the different fluxes. Note that per unit surface here means normalizing for the zy-plane, so for the surface going out of the paper of 3.3 and the corresponding per unit length then means per unit of the horizontal line of 3.3. The fluid flux and electric current per unit length are plotted in figure 5.1 to have a more insightful look at where the maximum fluxes are. For the fluid flux, plotted in figure 5.1a, it seems that the interference effects from a small channel length weigh much heavier than the interference effects from a small distance between channels: The most efficient way to let as much fluid flow through a membrane as possible, when L can still vary, is by having the channels as close to each other as possible and then finding a channel length that yields a maximum flux at this distance. To make this clear, consider figure 5.1a, $L = 0.2\mu$m clearly has a maximum flux per unit length that is lower than that of the maximum flux for greater channel lengths. So in this case it is advantageous to increase the channel length. For all channel lengths up to $L = 0.5\mu$m this argument can be made. For $L = 0.7\mu$m it can already be seen that the maximum fluid flux is found at a distance close to $S = W$, which is the minimal distance possible and for $L = 0.9\mu$m no maximum can be seen anymore in the fluid flux versus channel distance plot. But the maximum fluid flux is not much more than that of $L = 0.7\mu$m. Increasing the channel does not seem to increase the fluid flux much anymore after $L = 0.9\mu$m. At the beginning, when going from small channel lengths to greater channel lengths, the relief from the entrance interference effects has a more positive effect on the fluid flux than the negative effect of the decreasing salt concentration gradient, but after a certain point the channel length is long enough that entrance effects do not have a significant influence anymore and the decreasing salt concentration gradient becomes the more important factor.

Another very interesting observation from figure 5.1a is that the fluid flux starts to rise again for $L = 0.1\mu$m and $L = 0.2\mu$m for channel distances below $S = 2W$ and $S = 2W$ respectively. The cause for this can be seen in figure 5.3. For this it first must be noted that the fluid flux is derived as the average absolute value of the fluid velocity over a cross-section of the middle of the channel times the width of the channel. As discussed before in section 2.7 the EDL indirectly induces a fluid flow parallel to the surface. If the distance between the channels is large enough, the EDL on the curving surface pulls the fluid along with it. But when S becomes smaller there is less room for the fluid to be pulled around the corner and the fluid from both channels start blocking each other. For $L = 0.1\mu$m a critical point is reached at around $S = 2W$ at which the fluid is blocked that much by the other channels, that a circulation starts to occur. Where first the fluid could escape around the corner, the fluid is now pushed back around to the x-axis of the channel. The fluid flow magnitude parallel to the surface is maximum in the EDL. Maximum velociy means maximum fluid flux. This fluid flux has to come from somewhere, since the fluid is incompressible, following the continuity equation (2.2). When the distance between channels is large enough, this flux can curve around the corner from the reservoir into the channel and curve out from the channel around the corner of the inlet into the reservoir, but when the fluid can not curve around the corner of the inlet anymore, since the fluid flow is obstructed by the neighbouring channels,

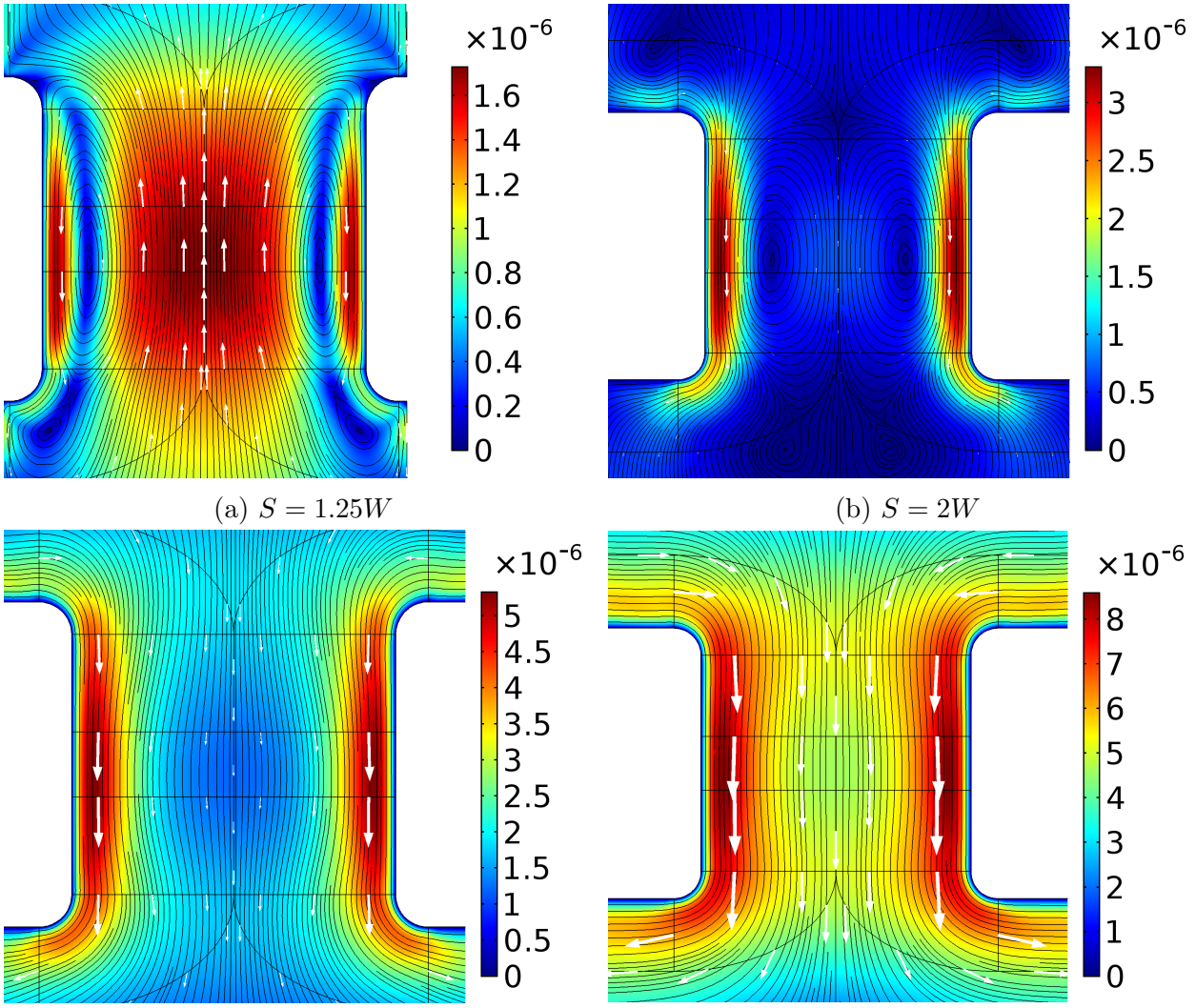

(a) $S = 1.25W$ (b) $S = 2W$

(c) $S = 3W$ (d) $S = 6W$

Figure 5.3: Fluid velocity surface plot in m/s with streamlines (black) and velocity vectors (white) for channel length $L = 0.1\mu$m for distances between channels: $S = 1.25W$, $S = 2W$, $S = 3W$ and $S = 6W$. With the surface charge extending all the way around the corner of the inlet.

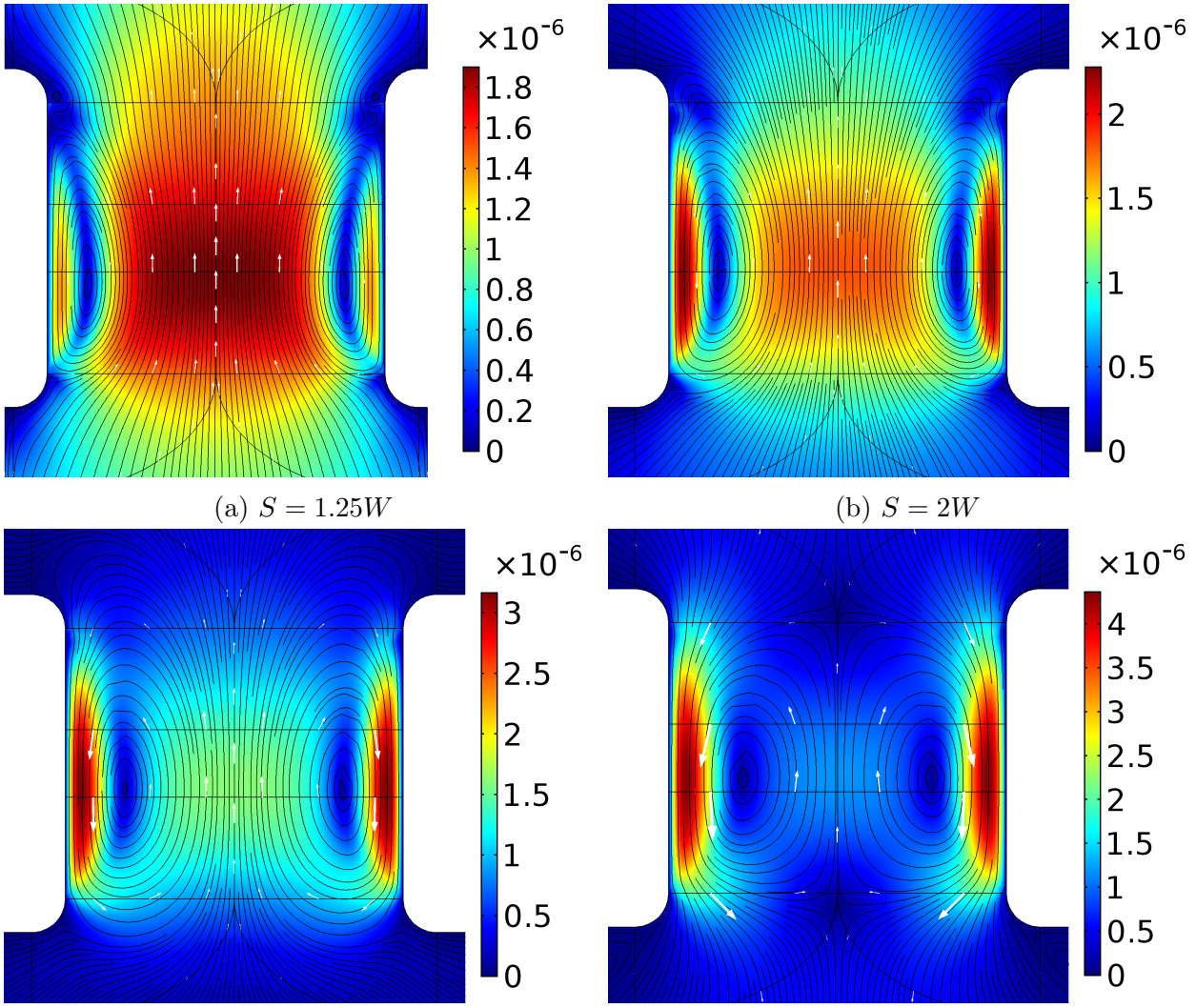

(a) $S = 1.25W$ (b) $S = 2W$

(c) $S = 3W$ (d) $S = 6W$

Figure 5.4: Fluid velocity surface plot in m/s with streamlines (black) and velocity vectors (white) for channel length $L = 0.1\mu$m for distances between channels: $S = 1.25W$, $S = 2W$, $S = 3W$ and $S = 6W$. With the surface charge only in the middle of the channel.

the flux going into the region of the EDL of the channel has to come from somewhere and the flux going out of the region of the EDL of the channel has to go somewhere. This flux excess at the EDL at the bottom outlet of the channel will complement the flux deficit at the EDL at the top inlet of the channel because the flux deficit and flux excess have worked up a pressure gradient in the opposite direction of the original flow from the salt concentration gradient. When reducing the distance between channels even further, this effect only enlarges. When the EDL is not extended all the way around the corner this effect occurs for all distances between channels, see figure 5.4 and the flow is suppressed much more than when the EDL is extending all the way around the corner. This can also be seen in figure 4.3. For large channel lengths this effect is less significant since entrance effect play much less of a role here in obstructing the fluid flow, but for small channel lengths the effect is really significant. The fluid flow is not pulled around the corner of the outlet when the surface charge does not extend all the way around the outlet leading to a significant suppression of the fluid flow and electric current.

For the electric current, plotted in figure 5.1b, it seems that an equilibrium is found between the impact of the in- or decreasing entrance interference and the in- or decreasing salt concentration gradient. Below a channel distance of $2.5W$ it is advantageous to increase the channel length when decreasing the distance between channels to yield a maximum electric current: the electric current is proportional to the channel length, this current will never be as high as the maximum current that can be reached at a distance of $2.5W$ though. Above a channel distance of $2.5W$ it is advantageous to decrease the channel length when increasing the distance between channels to yield a maximum current: the current is inversely proportional to the channel length, this current will also never be as high as the maximum current that can be reached at a distance of $2.5W$. There seems to be a combination of channel length and channel distance, that is not a combination where one of the two has to be minimal, that gives a maximum electric current! This equilibrium point is at a distance between channels of $S = 2.5W$ and at a channel length of $L = 0.3\mu$m.

The differences in positions of the maxima for the fluid flux and the electric current in figure 5.1 can be clarified by the backflow seen in 5.3 and 5.4. The electric current per distance between channels is at a maximum when the fluid velocity per distance between channels in the EDL region is at a maximum. For $L = 0.1\mu m$ this is the case at around $S = 3.5W$. But the fluid velocity is at a maximum when the fluid velocity per distance between channels across the whole channel is at a maximum. For the fluid flux this happens at greater distances between channels, because at a certain point, the interference from the neighbouring channels starts to slow down the flow in the middle of the channel, as explained earlier, but does not yet have an effect on the flow in the EDL. For larger channel lengths these entrance effects get smaller, which is exactly why for larger channel lengths the maxima of the fluid flux and the electric current are closer to each other, as seen in figure 5.1.

Thus far the fluid flux and the electric current have been normalized for the distance between channels but not yet for the length of the channels. To maximize the current per surface cross section, like the cross section in figure 3.3, the fluid flux and the electric current can be normalized by dividing it by the channel length. Realizing that the generated power is proportional to I^2. The shape of the generated power will look like 5.2b, with the actual generated power being only off by multiplicative factor. Here it can be seen that the generated power and the fluid flux are inverse proportional to the channel length. The channel distance

at which the generated power and the fluid flux are maximum is also inverse proportional to the channel length. The rise in fluid flux for small channel lengths and small distances that can be seen in figure 5.2a is due to the fact that the fluid flux is derived as the absolute value of the average velocity over a cross section of the channel. So in fact the actual fluid flux through the channel, which is outgoing minus ingoing flux, is going to zero for small channel lengths and distances between channels. Which can also be seen in figure 5.3.

6 Conclusion

A nanopre subjected to a pressure gradient or electric field in a system described by the parameters from table 1 will generate fluid- and net charge fluxes that are linear to their driving forces. This linear response is valid in a wide regime, which is for the pressure gradient at least from $\Delta p = 0.05$atm to $\Delta p = 0.5$atm and for the electric potential gradient at least from $\Delta V = 0.002$V to $\Delta V = 0.1$V. A nanopore subjected to a salt concentration gradient will generate a fluid- and net charge fluxes that are linear to their driving force in at least a regime of $\rho_{in}/\rho_{out} = 1.5$. When considering a chain of nanpores, a membrane, subjected to a driving force of $\rho_{in}/\rho_{out} = 1.2$ with the surface charge extending all the way around the corners of the in- and outlet, when the channel length can still be varied, a maximum fluid flux is found at minimal distance between channels and at a channel length of not more than $L = 1\mu m$. A maximum electric current is found at $S = 2.5W$ and $L = 0.3\mu m$. When the EDL does not extend around the corner, the fluid flow and electric current get obstructed resulting in much smaller fluxes. When also normalizing for the channel length, thus finding the maxima per volume element of membrane, the maximum fluxes per unit volume are found for minimum channel length, but for a finite distance between pores as seen in figure 5.2. Leaving as conclusion that the best porosity for a membrane, when considering RED, to maximize the generated power, is that of an as thinly possible shaped membrane with distances at the maxima found in figure 5.2b. This can be explained by the entrance effects obstructing the fluxes when the distance between channels is getting too small. The first priority in going further with research in this area is verifying the different linear response theory relations. It already has been shown by [8] that these relations hold, in the regimes considered in this thesis, for a cylindrical geometry, so there is no worry that this goal cannot be reached. Furthermore it should be verified whether or not the small distances between channels yield linear relations between the salt concentration gradient and the resulting fluxes. After that a theory for the entrance effects should be drawn up, since these effects are the main contributor to the interesting results that are found in this thesis. Also the optimal geometry found here, could be tested for different nanomaterials used in membranes for RED.

References

[1] Feng, J., Graf, M., Liu, K., Ovchinnikov, D., Dumcenco, D., Heiranian, M., Nandigana, V., Aluru, N., Kis, A. and Radenovic, A. (2016). *Single-layer MoS2 nanopores as nanopower generators.* Nature, 536(7615), pp.197-200.

[2] Kim, J., Kim, S. and Kim, D. (2013). *Energy harvesting from salinity gradient by reverse electrodialysis with anodic alumina nanopores.* Energy, 51, pp.413-421.

[3] Siria, A., Bocquet, M. and Bocquet, L. (2017). *New avenues for the large-scale harvesting of blue energy.* Nature Reviews Chemistry, 1(11).

[4] Logan, B. and Elimelech, M. (2012). *Membrane-based processes for sustainable power generation using water.* Nature, 488(7411), pp.313-319.

[5] Siria, A., Poncharal, P., Biance, A., Fulcrand, R., Blase, X., Purcell, S. and Bocquet, L. (2013). *Giant osmotic energy conversion measured in a single transmembrane boron nitride nanotube.* Nature, 494(7438), pp.455-458.

[6] Hsu, J., Su, T., Lin, C. and Tseng, S. (2019). *Power generation from a pH-regulated nanochannel through reverse electrodialysis: Effects of nanochannel shape and non-uniform H+ distribution.* Electrochimica Acta, 294, pp.84-92.

[7] Werkhoven, B., Everts, J., Samin, S., Roij, R. *Flow-Induced Surface Charge Heterogeneity in Electrokinetics due to Stern-Layer Conductance Coupled to Reaction Kinetics*, Physical Review Letters. 120. 10.1103, 2018.

[8] Werkhoven, B., personal communication, February-May 2019.

[9] Boon, W., personal communication, Fbruary-June 2019.

[10] Van Heijst, G., *Fysische Transportverschijnselen deel I*, -Collegedictaat 3BB90-, 2006.

[11] *http://mathworld.wolfram.com/Polylogarithm.html*

[12] Roij, R., *Soft Condensed Matter Theory*, 2019.

[13] Kirby, B. (2010). *Micro- and Nanoscale Fluid Mechanics.* Cambridge: Cambridge University Press.

[14] Li, D. (2004). *Electrokinetics in microfluidics.* Oxford: Academic.

[15] Fick, A. (1995). *On liquid diffusion.* Journal of Membrane Science, 100(1), pp.33-38.

[16] Kundu, P., Cohen, I., Dowling, D. and Tryggvason, G. (n.d.). *Fluid mechanics.*

[17] Mouterde, T. and Bocquet, L. (2018). *Interfacial transport with mobile surface charges and consequences for ionic transport in carbon nanotubes.* The European Physical Journal E, 41(12).

A Appendix

A.1 Laminar pipe flow

Even though the plane Poiseuille flow is very straightforward to consider it is not a very realistic configuration. Therefore now consider laminar flow through a long cylinder of radius R centered along the z-axis, or just Poiseuille flow. This flow is very similar compared to the plane Poiseuille flow. Since flow through a cylinder is considered, the Navier-Stokes equations in cylindrical coordinates are used [16]. The cylinder has radius R and is centered along the z-axis. Azimuthal symmetry implies that $u_\theta = 0$ and from axisymmetry follows $\partial/\partial\theta = 0$ and again assuming the fluid to be fully developed, u_z is not dependent on the z-coordinate. The continuity equation can be reduced to:

$$\frac{1}{r}\frac{\partial(ru_r)}{\partial r} + \frac{1}{r}\frac{\partial u_\theta}{\partial \theta} + \frac{\partial u_z}{\partial z} = 0, \tag{A.1}$$

to $\partial(ru_r)/\partial r = 0$. Together with the boundary condition $u_r(r = R) = 0$, it follows then that u_r must be zero along the whole cylinder. From the r-component of the Navier-Stokes equation now follows: $\partial p/\partial r = 0$, such that the pressure is only dependent on the z-coordinate. The z-component of the Navier-Stokes equation then reduces to:

$$0 = -\frac{dp}{dz} + \eta\left[\frac{1}{r}\frac{d}{dr}\left(r\frac{du_z}{dr}\right)\right], \tag{A.2}$$

with boundary conditions:

$$\begin{aligned} \left.\frac{du_z}{dr}\right|_{r=0} &= 0; \\ u_z|_{r=R} &= 0. \end{aligned} \tag{A.3}$$

Integrating equation (A.2)twice gives:

$$u_z(r) = -\frac{1}{4\eta}\frac{dp}{dx}(-r^2 + C_1 \ln r + C_2), \tag{A.4}$$

with integration constants C_1 and C_2, using the boundary conditions just given finally the velocity profile is obtained

$$u_z(r) = -\frac{1}{4\eta}\frac{dp}{dx}(R^2 - r^2), \tag{A.5}$$

which resembles laminar pipe flow reminiscent to the flow we have already seen with the plane Poiseuille flow, i.e. the fluid particles only move parallel to each other in layers concentric around the z-axis of the cylinder. This flow is called Poiseuille flow. The fluid volume flux in the z-direction, per unit length in the θ-direction is now given by:

$$Q_u = \int_0^R dr u_z(r) 2\pi r = -\frac{\pi}{8\eta}\frac{dp}{dz}R^4, \tag{A.6}$$

from which the average velocity in the pipe immediately follows as:

$$\overline{u}_z(r) = -\frac{\pi}{8\eta}\frac{dp}{dz}R^3, \tag{A.7}$$

which again allows us to write the velocity in the pipe as a function of the average velocity:

$$u_z(r) = 2\overline{u}_z(r)(1 - \frac{r^2}{R^2}), \tag{A.8}$$

the maximum velocity in the pipe can be found at $r = 0$ and is twice the average velocity of the fluid in the pipe.